Coordination Chemistry Reviews 255 (2011) 993–1015

Contents lists available at ScienceDirect

Coordination Chemistry Reviews

journal homepage: www.elsevier.com/locate/ccr

Review

Comparative molecular chemistry of molybdenum and tungsten and its relation to hydroxylase and oxotransferase enzymes

Richard H. Holm[a,*], Edward I. Solomon[b,**], Amit Majumdar[a], Adam Tenderholt[b]

[a] Department of Chemistry and Chemical Biology, Harvard University, 12 Oxford St., Cambridge, MA 02138, United States
[b] Department of Chemistry, Stanford University, Stanford, CA 94305, United States

Contents

ARTICLE INFO

Article history:
Received 20 August 2010
Accepted 19 October 2010
Available online 3 November 2010

Keywords:
Comparative properties
Molybdenum
Dithiolene complexes
Oxo transfer reactions
Tungsten

ABSTRACT

The similarities and differences in the fundamental coordination chemistry of molybdenum and tungsten mainly in physiological oxidation states M^{IV-VI} are examined in relation to the properties of enzyme sites that catalyze oxygen atom transfer reactions. The comparative aspects of dithiolene complexes, which as synthetic analogues simulate structural and electronic features of these sites, are emphasized. Analogue reaction systems of enzymes are summarized. The mechanism of reduction of the biological substrate Me_2SO in one such system as elucidated as with density functional calculations is presented as a case study.

Abbreviations[1]: Ad, adamantyl; BDE, bond dissociation energy; DMSOR, dimethylsulfoxide reductase; edta, ethylenediaminetetraacetate(4−); eu, cal deg^{-1} mol^{-1}; EXAFS, extended X-ray absorption fine structure; FMDH, *N*-formylmethanofuran dehydrogenase; FMO, frontier molecular orbital; M, molybdenum and/or tungsten; Me_3tacn, 1,4,7-trimethyl-1,4,7-triazacyclononane; py, pyridine; Q, O, S, Se; $R_2C_2S_2$, aliphatic or aromatic dithiolene (generalized); silox, tris(*tert*-butyl)silyloxide(1−); S_2pd, pyranopterindithiolate cofactor ligand (**1**); TMNOR, trimethylamine *N*-oxide reductase; XAS, X-ray absorption spectroscopy; XOR, xanthine oxidoreductase.

* Corresponding author. Tel.: +1 617 495 0853; fax: +1 617 496 9289.
** Corresponding author. Tel.: +1 650 723 9104.
E-mail addresses: holm@chemistry.harvard.edu (R.H. Holm), edward.solomon@stanford.edu (E.I. Solomon).

[1] For abbreviations see also Fig. 2. For ligand abbreviations in Table 4, consult the indicated references.

0010-8545/$ – see front matter © 2010 Elsevier B.V. All rights reserved.
doi:10.1016/j.ccr.2010.10.017

1. Introduction and scope

The pronounced similarity, and in some cases near-identity, of many molecular properties in the chemistry of molybdenum and tungsten follow from two principal factors: analogous valence electron configurations in all oxidation states of nearly all compounds, and virtually identical radii – atomic and ionic radii for a given oxidation state – arising from the lanthanide contraction. There also exist clear differences, some in reactivity such as variant polymerization (speciation) of oxo anions in aqueous solution [1,2] and others based on electronic structure such as ionization and redox potentials [3,4] and relativistic effects on structural properties [5]. The explosive growth in the understanding of the structure and function of molybdoenzymes [6–9] and the emergence and accelerating examination of tungstoenzymes [9–13] renders this an opportune time for comparison of the similarities and differences of these elements. We do so against a background of accumulated information and interpretation of properties of comparable sets of synthetic complexes of molybdenum and tungsten.

Because of space constraints, only certain concepts or properties relevant to enzyme sites that are manifested by molecular systems are considered. This treatment encompasses pertinent chemistry of the biological metal oxidation states 4+, 5+, and 6+; it does not include such extensive topics as lower oxidation state chemistry, metal–metal bonded systems and other polynuclear species, and organometallic chemistry. The large majority of examples are drawn from the chemistry of dithiolene complexes whose ene-1,2-dithiolato ligands provide stereochemical and electronic features credibly related to the immediate coordination enviroments of enzyme sites. As will be seen, such complexes have been profitably employed as site analogues [14–17]. Fortunately for comparative purposes, dithiolenes encompass by far the largest number of examples of isoelectronic isoligated pairs of molybdenum and tungsten complexes. This account proceeds through property comparisons and concludes with several case studies of dithiolene systems that convey detailed information pertinent to enzyme behavior. Data presented for various subjects are comprehensive and illustrative but not exhaustive.

2. Comparative atomic and molecular properties

2.1. Atomic and ionic properties

Selected properties, mainly of the neutral atoms, are compared in Table 1. Although estimates vary, molybdenum and tungsten are about equally abundant in the earth's crust, being the 54th and 55th most abundant elements. However, the concentration of molybdenum (as molybdate) in the oceans is several orders of magnitude larger than for tungsten. Indeed, molybdenum is the most abundant transition element in sea water and the 25th most abundant overall, and hence presents a greater potential bioavailability than tungsten. Molybdenum occurs in soil, water, plants, and animals to the extent of a few ppm. There are environments such the black smoker hydrothermal vents and sulfide-rich waters where tungsten concentrations are higher. In these locales hypthermophiles grow and incorporate tungsten in their enzymatic processes. Molybdenum and tungsten are the only elements in the second and third rows of transition elements that occur in native enzymes. Molybdenum has seven stable isotopes and tungsten five. Isotopes with non-zero nuclear spins normally afford hyperfine interactions useful in identifying and analyzing EPR spectra. ^{95,97}Mo NMR spectroscopy is a standard technique for many types of complexes [18,19], whereas ^{183}W NMR is much more difficult to implement by direct observation or indirect heteronuclear techniques because of long relaxation times and inherently low sensitivity. No molybdenum or tungsten NMR properties of proteins have been reported nor have Mössbauer spectra of tungstoenzymes. Becauses of high detection limits, the prognosis for biological tungsten Mössbauer spectroscopy is unpromising [13].

Electron affinities, several standard potentials [20], and higher ionization potentials (estimated for tungsten [3]) reveal the general tendency of easier oxidation of tungsten than molybdenum (vide infra). The lanthanide contraction, arising because the 4f electrons imperfectly screen the increasing nuclear charge in the lanthanide series (Z = 57–71) and from relativistic effects which affect screening after this series [5,21], affords practically equal atomic radii and nearly equal ionic radii for a given oxidation state. As will be

Table 1
Comparative properties of molybdenum and tungsten[a].

	Mo	W
Atomic number	42	74
Atomic weight	95.94	183.84
Abundance[b]		
Earth's crust	1000 μg/kg	1000 μg/kg
Ocean	1×10^{-7} pmolal	5×10^{-10} pmolal
Stable isotopes	^{92}Mo (14.84%), ^{94}Mo (9.25%), ^{95}Mo (15.92) ^{96}Mo (16.68%), ^{97}Mo (9.55%), ^{98}Mo (24.13%) ^{100}Mo (9.63%)	^{180}W (0.13%), ^{182}W (26.3%), ^{183}W (14.3%), ^{184}W (30.7%), ^{186}W (28.6%)
Ground electron configuration	[Kr]4d^{5}5s^1	[Xe]4f^{14}6s^{2}5d^4
Ground state	$^7S_3$	$^5D_0$
Isotopes with non-zero nuclear spins	^{95,97}Mo (I = 5/2)	^{183}W (I = 1/2)
1st ionization energy	7.0995 eV	7.980 eV
Electron affinity (M → M$^-$)	0.746 eV	0.815 eV
Standard potential E^0: $[MO_4]^{2-}$/M^0 [e]	−0.913 V	−1.074 V
Atomic radius	1.36 Å	1.37 Å
Pauling electronegativity	2.16	2.36
Mössbauer nuclei	–	W^{182}
Biol. oxidation states	4+ (4d^2), 5+ (4d^1), 6+ (4d^0)	4+ (5d^2), 5+ (5d^1), 6+ (5d^0)
Ground state spin	3+ (3/2)[d] 4+ (0), 5+ (1/2), 6+ (0)	Same as Mo
Shannon radii[c] (CN), A	3+ (6) 0.83	–
	4+ (6) 0.79	4+ (6) 0.80
	5+ (4) 0.60, (6) 0.75	5+ (6) 0.76
	6+ (4) 0.55, (5) 0.64, (6) 0.73	6+ (6) 0.74

[a] For these and other data, *cf.* J. Emsley, "The Elements", Oxford University Press, 3rd ed., 1998.
[b] Cox, "The Elements, Their Origin, Abundance, and Distribution", Oxford University Press, 1989.
[c] R.D. Shannon, Acta Crystallogr. A32 (1976) 751–767.
[d] Octahedral.
[e] Basic or neutral solution.

Table 2
Pairs of molydenum and tungsten dithiolene complexes and properties reported.

Complexes[a]	Properties[b]	Refs.
$[M^{VI}L_2L'(S_2C_2R_2)]^{1-}$		
$[M^{VI}O_3(bdt)]^{1-}$	A, IR, NMR, XR	[23]
$[M^{VI}O_3(3,6\text{-}Cl_2bdt)]^{1-}$	IR, NMR, XR	[24]
$[M^{VI}O_2(OSiR_2R')(bdt)]^{1-}$	A, E, IR, NMR, XR	[23,25,26]
$[M^{IV/V}Q(S_2C_2R_2)_2]^{2-/1-}$		
$[M^{IV}O(mnt)_2]^{2-}$	A, E, IR, RR, XR	[27–30] [31–35]
$[M^{IV}O(tfd)_2]^{2-}$	IR, NMR, XR	[36]
$[M^{IV}O(mdt)_2]^{2-}$	A, E, IR, NMR, XR	[34,37,38]
$[M^{IV}O(bdt)_2]^{2-}$	A, E, IR, NMR, XR	[29,39–43] [33,34,44]
$[M^{V}O(bdt)_2]^{1-}$	A, E, RR, XAS, XR	[33,39,41,45,46]
$[M^{IV}O(S_2C_2(CO_2Me)_2)_2]^{2-}$	A, E, IR, NMR, RR, XR	[27,29,32,47]
$[M^{IV}O(fdt)_2]^{2-}$	A, E, IR, NMR, XR	[34]
$[M^{IV}S(mdt)_2]^{2-}$	A, E, NMR, XR	[38,49]
$[M^{IV}Se(S_2C_6H_8)_2]^{2-}$	A, E, IR, XR	[50]
$[M^{IV}(QR)(S_2C_2R_2)_2]^{1-}$		
$[M^{IV}(OR)(mdt)_2]^{1-}$	A, NMR, XR	[51–56]
$[M^{IV}(OPh)(pdt)_2]^{1-}$	A, NMR, XR	[52,53]
$[M^{IV}(OC_6H_4\text{-}p\text{-}X)(mdt)_2]^{1-}$	A, NMR, XR	[53,57]
$[M^{IV}(OC_6H_2\text{-}2,4,6\text{-}Pr^i_3)(mdt)_2]^{1-}$	A, NMR	[58]
$[M^{IV}(OSiPh_2Bu^t)(bdt)_2]^{1-}$	A, IR, NMR, XR	[42,43,59]
$[M^{IV}(O_2CR)(mdt)_2]^{1-}$	A, IR, NMR, XR	[38,51,60]
$[M^{IV}(SC_6H_2\text{-}2,4,6\text{-}Pr^i_3)(mdt)_2]^{1-}$	A, NMR, XR	[60,37]
$[MLL'(S_2C_2R_2)_2]^{0/1-/2-}$		
$[M(CO)_2(mdt)_2]$	A, IR, NMR, XR	[37,61–64]
$[M(CO)_2(pdt)_2]$	A, IR	[37,62,61]
$[M^{IV}(CO)(SPh)(mdt)_2]^{1-}$	A, IR, NMR, XR	[56,37]
$[M^{IV}(CO)(SeR)(mdt)_2]^{1-}$	A, IR, NMR, XR	[56,37]
$[M^{IV}(PMePh_2)_2(bdt)_2]$	A, NMR, XR	[65] [66,67,43]
$[M^{VI}O_2(S_2C_2R_2)_2]^{2-}$		
$[M^{VI}O_2(mnt)_2]^{2-}$	A, E, IR, NMR, RR, XR	[28,29,68,69]
$[M^{VI}O_2(bdt)_2]^{2-}$	A, E, IR, NMR, RR, XR	[29,59,68,70,71]
$[M(S_2C_2R_2)_3]^{0/1-/2-}$		
$[M(edt)_3]$	A, E, XR	[72–74]
$[M(mnt)_3]^{2-}$	E, IR, XR	[28,75,76,30]
$[M(mdt)_3]^{0/1-/2-}$	A, E, XR	[37,64,73,74,77]
$[M(tfd)_3]^{0/1-/2-}$	E, EPR, IR, NMR, XR	[78,79,36]
$[M(S_2C_3S_3)_3]^{1-/2-}$	E, EPR, XR	[80,81]
$[M(pdt)_3]^{0/1-/2-}$	A, E, EPR	[73,74,77,82]
$[M(S_2C_2HPh)_3]$	E, IR, NMR, XR	[82–84]
$[M(bdt)_3]^{0/1-/2-}$	A, E, XR	[77,85–87,67,88,89]
$[M(tdt)_3]^{0/1-}$	A, E, EPR	[75,77]
$[M(3,5\text{-}Bu^t_2bdt)_3]^{0/1-}$	A, IR, E, XAS, XR	[90]
$[M(3,6\text{-}Cl_2bdt)_3]^{0/1-/2-}$	XR	[91]
$[M(Cl_4bdt)_3]^{0/1-/2-}$	A, E, EPR	[75,92,93]

[a] R,R′ are generalized alkyl and/or aryl substituents. X = Br, Me, OMe, COMe.
[b] A, absorption spectrum; E, redox potentials; IR, infrared spectra; RR, Raman or resonance Raman spectra; XAS, X-ray absorption spectra; XR, X-ray structure. References include preparations of compounds.

seen, structures of molecules with the same ligands in each of the three established biological oxidation states are effectively constant, but certain properties such as redox potentials adhere to an order foreshadowed by the results in Table 1.

2.2. Dithiolene complexes and property comparisons

In the sections that follow, data on certain molecular properties are assembled for purpose of comparison between molybdenum and tungsten molecules. While diverse molecular types are included, examples are largely dithiolene complexes. Sections 4 and 5 deal exclusively with dithiolenes. Consequently, dithiolene complexes are introduced at this point with the aid of Table 2, which lists some 38 comparative pairs distributed over six generalized structure types. Principal structure types are depicted in Fig. 1 and ligands in Fig. 2. While the non-innocent behavior of dithiolenes is well documented (including molybdenum and tungsten)

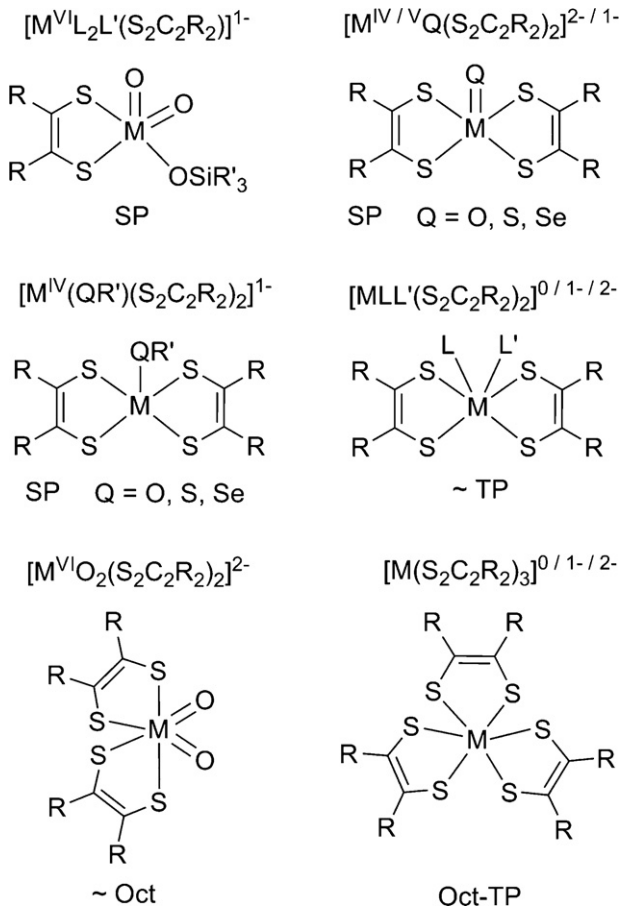

Fig. 1. Schematic depictions of the six general structural types of Mo/W complexes comprising the comparative pairs in Table 2. Such complexes are isoelectronic and have identical ligands and closely corresponding structures. Idealized stereochemistry: SP, square pyramidal; TP, trigonal prismatic; Oct, octahedral; Oct-SP, intermediate between the two limits. Here and elsewhere, the formula $(S_2C_2R_2)^{2-}$ is a general designation of ethylenic and aromatic dithiolate ligands.

[22], these ligands function in the classical ene-1,2-dithiolate or benzene-1,2-dithiolate forms in enzyme site analogues and, insofar as known, in the sites themselves. Metals are coordinated by the pyranopterindithiolate cofactor ligand **1** (S_2pd), also shown in Fig. 2.

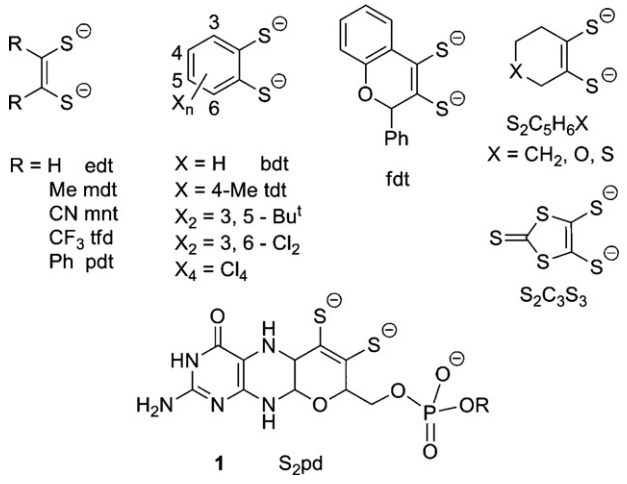

Fig. 2. Definition of dithiolate ligand structures and the pyranopterindithiolate cofactor ligand (**1**, R absent or a nucleotide).

Table 3
Bond length comparisons in isoligated molybdenum and tungsten complexes.

Symmetry[a]	Complex	Mo, W bond lengths (Å)	Refs./ref code[b]
T_d	$[M^{VI}O_4]^{2-}$	1.764[8], 1.760[4]	BAGPEE01, PEHLUJ
	$[M^{VI}S_4]^{2-}$	2.180[7], 2.195[8]	ADEGEW, TITQUJ
O_h	$[M^{VI}F_6]$	1.817[2], 1.826[1]	[d]
	$[M^{IV}Cl_6]^{2-}$	2.355[2], 2.347(5)	[e]
D_{3h}	$[M^{VI}Me_6]$[c]	2.11[1], 2.19[2]; 2.107[9], 2.19[1]	LOGDIX, ZOSXEK01
D_{3h}/O_h	$[M(bdt)_3]^{2-}$	2.39(1), 2.391(8)	[59,89]
C_{4v}	$[M^{IV}OCl_4]^{2-}$	M–Cl: 2.34[2], 2.379[1] M=O: 1.646(2), 1.676(3)	LIMRUU, COYWAO
	$[M^{IV}O(mdt)_2]^{2-}$	M–S: 2.388[1], 2.379[3] M=O: 1.712(2), 1.741(2)	[37,62]
	$[M^{IV}S(S_2C_2R_2)_2]^{2-}$ [f]	M–S: 2.362[7], 2.348[3] M=S: 2.172(2), 2.162(2)	[49,62]
	$[M^{IV}Se(S_2C_6H_8)_2]^{2-}$	M–S: 2.360[6], 2.355[6] M=Se: 2.307(1), 2.314(1)	[50]
	$[M^{IV}(OMe)(mdt)_2]^{1-}$	M–S: 2.33[1], 2.33[1] M–O: 1.862(3), 1,824(5)	[51]
	$[M^{IV}(SR)(mdt)_2]^{1-}$ [g]	M–S: 2.31[7], 2.313[5] M–SR: 2.338(1), 2.319(1)	[60,37]
C_{3v}	$[M^{VI}S_3(SBu^t)]^{1-}$	M=S: 2.341(2), 2.323(1) M–S: 2.148[1], 2.148[1]	[102]
C_{2v}	$[M^{IV}(O_2CR)(mdt)_2]^{1-}$ [h]	M–O: 2.20(1), 2.178(6) M–S: 2.332[6], 2.328[6]	[51,60]
	$[M(CO)_2(mdt)_2]$[i]	M–C: 2.025[3], 2.030[4] M–S: 2.380[1], 2.376[2]	[37,62]
C_2	$[M^{VI}O_2(mnt)_2]^{2-}$	M–S: 2.439(2), 2.445(2) M–S[j]: 2.635(3), 2.622(3) M=O: 1.721(6), 1.701(6)	[30,68]

[a] Actual or idealized coordination sphere symmetry.
[b] Cambridge Structural Database.
[c] C_{3v} distortion.
[d] T. Drews, J. Supel, A. Hagenbach, K. Seppelt, Inorg. Chem. 45 (2006) 3782–3788.
[e] B. Hu, P. Wang, Y. Xiao, L.-P. Song, Z. Krist. NCS 220 (2005) 298; W. Xu, Y.-Q. Zheng, Z. Krist. NCS 220 (2005) 323.
[f] R = Me, Ph.
[g] R = 2,4,6-$Pr^i_3C_6H_2$.
[h] R = Me, Ph.
[i] M oxidation state ambiguous.
[j] Trans to oxo in distorted octahedral structure.

2.3. Stereochemistry and structural and metric features

Collected in Table 3 are comparisons of bond distances in isoligated $M^{IV,V,VI}$ complexes in a variety of stereochemical arrangements. Examples include relatively symmetric species chosen because of smaller variations in individual parameters of a given molecule but of course do not avoid the imprecision encountered with comparisons of metric parameters from independent determinations, some at different temperatures. Nonetheless, the data substantiate nearly equal bond lengths for a given oxidation state and ligand donor atom.

Most values are the same based on the usual 3σ criterion. In our experience, apparent differences in bond lengths normally do not exceed 0.05 Å and are usually less. The tabulation also provides a convenient list of bond lengths that may be expected to apply to protein sites. For example, consider the structural comparison between the oxidized sites and synthetic compounds in Fig. 3. Protein site bond lengths were determined by EXAFS analysis; other values are from X-ray structures. The structure of square pyramidal $[WO_2S(bdt)]^{2-}$ [24] reveals the differing trans influence of oxo and sulfido on W–S_{bdt} distances which was not detectable by EXAFS [94]. The structure of $[WO(OMe)(mdt)_2]^{1-}$ is intermediate between octahedral and trigonal prismatic and shows a trans oxo effect. Otherwise, bond distances of the oxidized DMSOR site and a synthetic analogue are within the expected range. A similar relationship exists with the oxidized site of *E. coli* DMSOR [95]. The comparisons necessarily involve tungsten complexes because their molybdenum analogues are unstable and have not been isolated. Note that a substantial database of XAS results for synthetic molybdenum and tungsten complexes has been accumulated for the purpose of characterizing and refining metric features of enzyme sites [96–98].

There is a limited number of cases where metal–ligand bond lengths are appreciably different, sometimes with accompanying intermolecular interactions. Consider, for example, the isomorphous pair of nitrido complexes $[M^{VI}N(OBu^t)_3]$ [99,100]. These compounds are linear polymers with chain-like M≡N···M interactions and nitrogen atoms in the apical positions of a trigonal

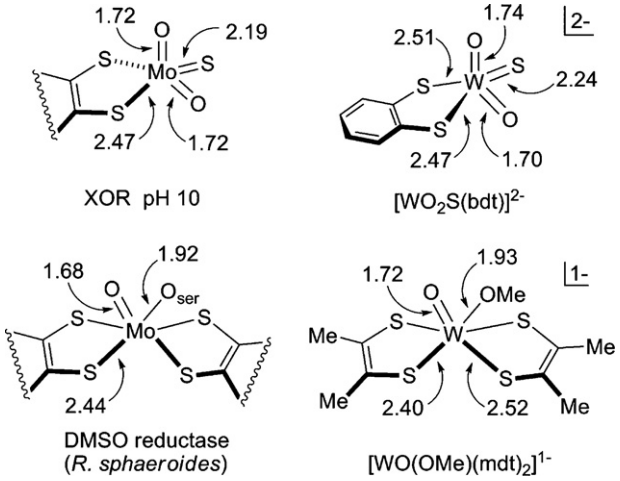

Fig. 3. Schematic structures and bond lengths (Å) of the oxidized sites in bovine XOR at pH 10 and wild-type *R. sphaeroides* DMSOR and in structural analogues; bond lengths were obtained from EXAFS and crystallographic data, respectively.

Table 4
Bond dissociation energies.

Bond	Complex	BDE (kcal/mol)[e]	Refs.
M^0–CO	$[M(CO)_6]$	41[a], 40[b] (Mo); 46[a], 44[b] (W)	[103,104]
M^I–CO	$[M(CO)_6]^{1+}$	33[a] (Mo), 36[a] (W)	[105]
M^0–PH_3	$[M(CO)_5(PH_3)]$	31[b] (Mo), 34[b] (W)	[106]
M^0–PMe_3	$[M(CO)_5(PMe_3)]$	38[b] (Mo), 44[b] (W)	[106]
M^0–PPh_3	$[Mo(CO)_4(PPh_3)_2]$	30[d]	[107]
M^I–PH_3	$[(C_5H_5)Mo(PH_3)_3]$	24[b]	[108]
M–SPh[g]	$[M(SPh)(CO)_3(PPr^i_3)_2]$	38[a] (Mo), 44[a] (W)	[109]
M–SePh[g]	$[M(SePh)(CO)_3(PPr^i_3)_2]$	34[a] (Mo), 39[a] (W)	[109]
Mo^I–QPh	$[Mo(QPh)(N[Bu^t]Ar)_3]$	55 (Q = S), 52 (Q = Se)	[109]
M^{II}–PH_3	$[(C_5H_5)MoH(PH_3)_3]$	24[b,c]	[108]
W^{IV}=O	$[WOCl_2(PMePh_2)_3]$	>138[f]	[110]
M^{IV}=O	$[(MeC_5H_4)_2MO]$	112[a] (Mo), 132[a] (W)	[111]
Mo^{IV}–$OPMe_3$	$[(Tp^*)MoOCl(OPMe_3)]$	30[a]	[112]
Mo^{VI}≡N	$[MoN(N[Bu^t]Ar)_3$	155[a]	[113]
Mo^{VI}≡P	$[MoP(N[Bu^t]Ar)_3$	92[a]	[114]
Mo^{VI}≡N–CN	$[Mo(OC[Ad]mes)_4(NCN)]$	104[a]	[115]
W^{VI}–F, W^V–F, W^{IV}–F	$[WF_6]$, $[WF_5]$, $[WF_4]$	111[b], 94[b], 123[b]	[116]
Mo^V=O	$[MoO(N[C(CD_3)_2Me]Ar)_3]$	156[a]	[117]
Mo^V=S	$[MoS(N[C(CD_3)_2Me]Ar)_3]$	104[a]	[117]
	$[MoS(N[Bu^t]Ar)_3]$	102[a]	[118]
Mo^V=Se	$[MoSe(N[Bu^t]Ar)_3]$	77[a]	[118]
Mo^{VI}=O	$[MoO_2(S_2CNEt_2)_2]$	95[a], 98[a]	[119]
M^{VI}≡O	$[MOCl_4]$	101[a],126[b] (Mo) 127[a], 145[b] (W)	[120,121]
M^{VI}≡S	$[MSCl_4]$	79[b] (Mo), 103[b] (W)	[121]
M^{VI}≡Se	$[MSeCl_4]$	67[b] (Mo), 87[b] (W)	[121]

[a] Experimental value.
[b] Theoretical value.
[c] Values strongly dependent on X and singlet or triplet ground state in the series $[(C_5H_5)MoX(PH_3)_3]$.
[d] ΔH^i for phosphine dissociation of cis isomer.
[e] For additional data on organometallic compounds, *cf.* J. A. Martinho-Simões, J. L. Beauchamp, Chem. Rev. 90 (1990), 629–688.
[f] Estimated value.
[g] Ligand radical complexes.

bipyramid. Intramolecular M≡N bonds are appreciably different (Mo 1.664(1) Å, W 1.74(2) Å) while M–O bond lengths are the same. The effect is ascribed to W^{VI} being a weaker oxidant and less prone to remove charge from the nitride. Consequently, the more basic nitride renders the W···N interaction (2.66(2) Å) stronger than the Mo···N interaction (2.88(1) Å). Because the structures of discrete molecules are unavailable, it is not known whether the differing M≡N bond lengths are intrinsic or a consequence of the weak intermolecular interactions. The effect may be confined to very electron-rich nitrido ligand; similar behavior with M=O or M=S bonds has not been described.

With the exception of occasional minor differences in bond angles, the stereochemistry of isoligated isoelectronic molybdenum and tungsten molecules is the same. Recently, an instructive exception to this regularity has been demonstrated in the form of the four-coordinate complexes $[M^{IV}(silox)_3Cl]$ (**2**, **3**) shown in Fig. 4. Complex **2** has a distorted trigonal monopyramidal shape while **3** presents a flattened tetrahedral geometry. Further, **2** has a triplet ground state with a $[4d_{xz,yz}]^2$ configuration, calculated to be *ca.* 11 kcal/mol below the singlet state $[4d_{z^2}]^2$. Complex **3** has a singlet ground state $[5d_{z^2}]^2$ almost equienergetic with a triplet state $[5d_{xz,yz}]^2$. The effect has been traced to greater stability of the $5nd_{z^2}$-type orbital of tungsten because of larger $nd_{z^2}/(n+1)s$ mixing in the third row of transition elements [101]. This behavior is unlikely to occur (and has not been detected) in five- or six-coordinate protein sites and dithiolene complexes where geometry favors occupancy of an in-plane d-orbital (d_{xy}) often normal to a strong axial ligand field component such as that furnished by oxo ligands and approximately non-bonding.

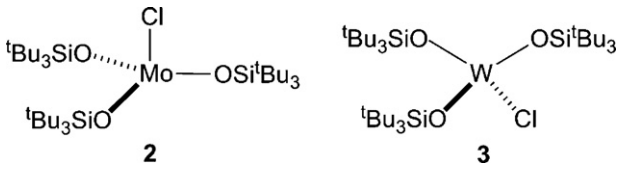

Fig. 4. Schematic structures of $[M(silox)_3Cl]$. M–O 1.869(4) Å (Mo), 1.865(8) Å (W); M–Cl 2.298(1) Å (Mo), 2.338(1) Å (W); O–M–O 115.6° (Mo), 2 at 101°, 1 at 148.2° (W); O–M–Cl 2 at 104.2°, 1 at 98.6° (Mo), 2 at 89.2°, 1 at 139.7° (W).

From a consideration of an extensive body of structural data, the following generalization emerges.

- *Isoelectronic isoligated five- and six-coordinate complexes of Mo^{IV-VI} and W^{IV-VI} are isostructural and nearly isometric.*

2.4. Bond energies

Bond dissociation energies for a variety of complexes are collected in Table 4, including eight pairs of isostructural isoelectronic complexes. Here low-valent organometallic compounds are included in order to provide a full range of BDEs. The results were obtained in two ways. Experimental values derive from thermochemical measurements on the molecules in question or their precursors, often with ancillary experimental enthalpy data utilized in an additive or cyclic manner to evaluate the desired bond energy. Theoretical values result from computational investigations based on various DFT approaches. Suggested uncertainties in the original reports are sometimes given for theoretical values, and are often large for experimental values owing to error propagation when multiple data are required. The original literature should be consulted. Theory and experiment are sometimes in good agreement, the best examples being $[M(CO)_6]$ where results differ by only 1–2 kcal/mol. The lowest BDEs involve dissociation of a neutral ligand from a low (non-physiological) oxidation state. Current data for M^{0-II} carbonyl and phosphine complexes place these values in the 20–50 kcal/mol range. Higher oxidation states develop

stronger bonds, with the exception of the Mo^{IV}–$OPMe_3$ bond whose dissociation involves neutral components.

The data are perhaps most important in the recognition of BDE trends in $M^{IV–VI}$ complexes containing multiply bonded ligands Q. Particularly useful in this regard are the $Mo^{V,VI}$ complexes containing the bulky imido ligands $(N[R]Ar)^{1-}$ exploited so effectively by Cummins and coworkers [113–115,117,118] and DFT calculations on the $[M^{VI}QCl_4]$ C_{4v} series by Ziegler and coworkers [121]. Note that in Mo^{VI} and W^{VI} complexes with one Q ligand, M≡Q triple bonds arise by interaction of M d_{z2} and $d_{xz,yz}$ orbitals with p_σ and p_π orbitals of Q (M–Q vector is the *z*-axis). Two significant trends in BDEs follow below. There are no exceptions to the first trend, which does not arise from bond length differences, some of which are nearly identical in comparative pairs. In the optimized geometries of the $[M^{VI}QCl_4]$ series, for example, W≡Q bonds are apparently longer than Mo≡Q bonds by 0.029–0.038 Å. Other interesting issues, such as bond strengths as dependent on oxidation state at parity of ligation and structure and the influence of trans ligands at constant oxidation state in the same overall structure, cannot yet be addressed owing to the lack of necessary BDE and bond length data.

- *$BDE_W > BDE_{Mo}$ at constant oxidation state and ligation.*
- *At constant oxidation state and ligation, $BDE_O > BDE_S > BDE_{Se}$ for multiple bonds M–Q and $BDE_N > BDE_P$ for multiple bonds M–N and M–P.*

2.5. Redox potentials

Assembled in Table 5 are over thirty comparisons of redox couples covering the oxidation states $M^{III–VI}$. Component members of each pair are isostructural and isoelectronic. This list is restricted to mononuclear species and substantially expands previous data tabulations dealing with comparative potentials [4,34,122–124]. The results are given as differences ΔE in potentials of chemically reversible processes which were determined under the same (or nearly the same) experimental conditions in non-aqueous media. The large majority of data refer to dithiolene complexes. All ΔE values are positive, signifying that the tungsten member of each pair is

Table 5
Redox potential differences of selected molybdenum and tungsten complexes.

Couple	Ox. states	$\Delta E = E_{Mo} - E_W$ (mV)[h]	Refs.
$[MF_6]^{0/1-}$	6+/5+	1010[a,b]	[122]
$[MOCl_5]^{1-/2-}$	6+/5+	750[c]	[123]
$[MNCl_4]^{1-/2-}$	6+/5+	680[c]	[123]
$[MCl_6]^{0/1-}$	6+/5+	610[c]	[123,125]
$[MO(SR)_4]^{0/1-}$	6+/5+	240[d], 270[e,f]	[126]
$[MO(mdt)_2]^{0/1-}$	6+/5+	200[b]	[38,37]
$[MF_6]^{1-/2-}$	5+/4+	980[a,b]	[122]
$[MOCl_5]^{2-/3-}$	5+/4+	750[c]	[123]
$[MCl_6]^{1-/2-}$	5+/4+	650[c]	[123,125]
$[MO(Me_3tacn)Cl_2]^{1+/0}$	5+/4+	620[b]	[127,128]
$[MO(mdt)_2]^{1-/2-}$	5+/4+	290, 590[b]	[34,38,37]
$[MO(bdt)_2]^{1-/2-}$	5+/4+	280, 520[b]	[34,39]
$[MO(SR)_4]^{1-/2-}$	5+/4+	250[d], 270[e,f]	[126]
$[MS(mdt)_2]^{1-/2-}$	5+/4+	240[b]	[38,49]
$[MO(mnt)_2]^{1-/2-}$	5+/4+	180[b]	[34]
$[MO(fdt)_2]^{1-/2-}$	5+/4+	30[b]	[34]
$[MCl_6]^{2-/3-}$	4+/3+	870[c]	[123,125]
$[M(Me_3tacn)Cl_3]^{1+/0}$	4+/3+	840[b]	[127,128]
$[M(Tp)Cl_3]$	4+/3+	820	[129]
$[M(OPh)(mdt)_2]^{1-/2-}$	4+/3+	290[b]	[56]
$[M(mnt)_3]^{2-/3-}$	4+/3+	270, 370[b,c]	[75,76]
$[M(edt)_3]^{0/1-}$	[g]	43[f]	[74]
$[M(mdt)_3]^{0/1-}$	[g]	26[f]	[74]
$[M(tfd)_3]^{0/1-}$	[g]	70[b]	[78]
$[M(pdt)_3]^{0/1-}$	[g]	50[f]	[74]
$[M(tdt)_3]^{0/1-}$	[g]	28[f]	[77]
$[M(3,5\text{-}Bu^t_2bdt)_3]^{0/1-}$	[g]	10[c]	[90]
$[M(mnt)_3]^{1-/2-}$	[g]	60, 70, 100[b,c]	[75,76]
$[M(edt)_3]^{1-/2-}$	[g]	100[f]	[74]
$[M(mdt)_3]^{1-/2-}$	[g]	67[f]	[74]
$[M(tfd)_3]^{1-/2-}$	[g]	40[b]	[78]
$[M(pdt)_3]^{1-/2-}$	[g]	67[f]	[74]
$[M(tdt)_3]^{1-/2-}$	[g]	180[f]	[77]
$[M(3,5\text{-}Bu^t_2bdt)_3]^{1-/2-}$	[g]	120[c]	[90]

[a] W potential at 293 K, Mo potential at 273 K.
[b] Acetonitrile.
[c] Dichloromethane.
[d] R = 2,3,4,5-Me_4C_6H.
[e] R = 2,4,6-$Pr^i_3C_6H_2$.
[f] DMF.
[g] Ambiguous oxidation state(s).
[h] For additional data, *cf.* Ref. [124].

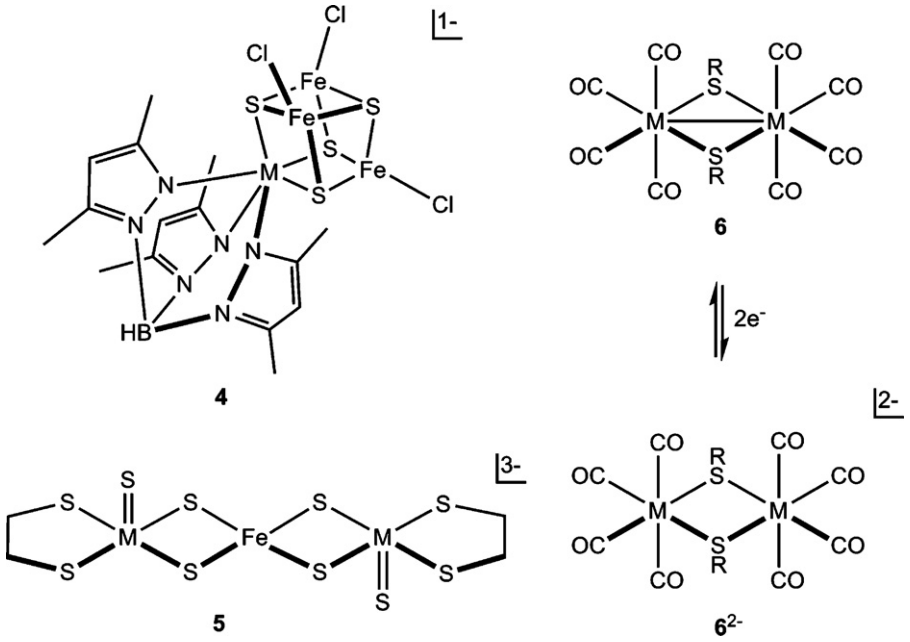

Fig. 5. Cubane-type $[(Tp^*)MFe_3S_4Cl_3]^{1-}$ (**4**), linear cluster $[M_2FeS_6(S_2C_2H_4)_2]^{3-}$ (**5**) and the two-electron redox couples $[M_2(SR)_2(CO)_8]^{0/2-}$ (**6**/$\mathbf{6}^{2-}$).

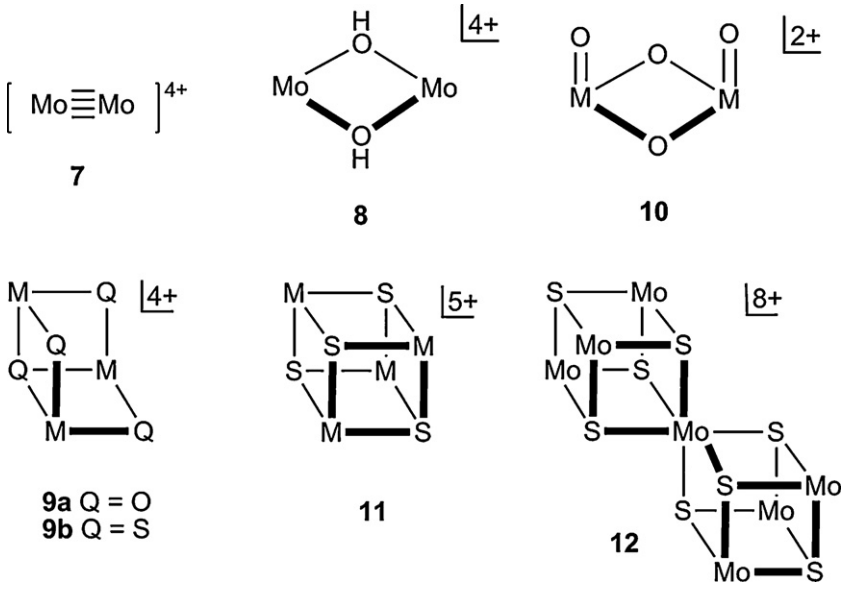

Fig. 6. Core structures of aqua ions **7**, **8** and **10** and sulfidoaqua ions **9**, **11** and **12**. Bound water molecules rendering each metal site five-coordinate (**7**) or six-coordinate (**8**–**12**) are omitted.

thermodynamically more readily oxidized (or less readily reduced) than its molybdenum counterpart. The largest potential differences occur in $M^{IV–VI}$ complexes with the more electronegative, less polarizable ligands as in halide, oxo, and nitrogen-bound cases. Values of ΔE maximize with $[MF_6]^{0/1-}$ (1010 mV) and $[MF_6]^{1-/2-}$ (980 mV). Introduction of thiolate and dithiolene ligation reduces nearly all ΔE values to below 300 mV. In the tris(dithiolenes), values for the 1−/2− couples are 180 mV or (usually) less and for 0/1− couples these values are below 100 mV. In the latter cases, the redox events are largely ligand-based, with the result that the intrinsic potential order of molybdenum and tungsten is maintained but with generally reduced potential differences.

The same potential order usually holds with metal clusters containing one or more molybdenum or tungsten atoms. Recent examples are the 1−/2− couples of cubane-type clusters **4** in Fig. 5 for which ΔE = 230 V in acetonitrile [130]. The clear implication is that the redox-active orbitals possess some M character even if, as shown with many $[MoFe_3S_4]^{3+/2+}$ core redox processes, the major changes in electron density upon oxidation or reduction occur in the Fe–S portion of the cluster. However, for the linear clusters **5** containing two M^V and one Fe^{III} atom in the isolated trianion, ΔE = 20 mV in Me_2SO for the 2−/3− couple [131]. This small separation suggests highly covalent and delocalized bonding at the M sites; iron-localized oxidation is not likely in view of the probable instability of Fe^{IV} in a tetrasulfido environment. We also note that the two-electron redox couples **6**/$\mathbf{6}^{2-}$ in acetonitrile or DMF present ΔE values almost all of which are nearly zero or are inverted with small negative values [132]. Oxidation is accompanied by M–M bond formation (formally $2Mo^0 \rightarrow M^I–M^I$); redox steps have been analyzed in detail [133]. These reactions combine low oxidation states and strongly covalent bonding that attentuates periodic differences in electron affinities between molybdenum and tungsten, a dual circumstance not encountered in biological systems.

The following generalization applies to redox potentials:

- *For $M^{VI/V}$, $M^{V/IV}$, and $M^{IV/III}$ redox couples of isoligated isostructural complexes, $E_{Mo} > E_W$ under the comparable experimental conditons, with the potential difference ΔE decreasing as the metal–ligand bond covalency increases.*

3. Solution chemistry and reactivity

3.1. Species in aqueous solution

The natural abundance and speciation of molybdenum and tungsten in water is obviously relevant to their bioavailabililty and incorporation into natural products. Frost and Pourbaix (*E*–pH) diagrams are often useful in describing solution behavior as are other speciation diagrams that present percentages or concentrations of different species as a function of pH at constant metal concentration or varying metal concentration at constant pH. Such diagrams and *E*–pH plots are available for these elements [1,2,134,135] and reveal that the most obvious similarity between the two elements when fully oxidized is their complexity below pH ∼ 6. At and above this value the dominant species are $[MO_4]^{2-}$, which have nearly the same first protonation constant: $\log K_1$ = 3.4–3.6 (Mo) [136], 3.5 (W) [137]. When concentrated solutions are made strongly acidic, yellow molybdic acid ($MoO_3 \cdot 2H_2O$) or white tungstic acid ($WO_3 \cdot 2H_2O$) precipitates. Structures of these materials have not been established. In dilute acidic solutions ($\lesssim$1 mM) the acids are sometimes written as H_2MO_4. Recent spectroscopic and theoretical results indicate that aqueous molybdic acid is based on the formulation $MoO_3 \cdot nH_2O$ with n = 3 providing the best agreement with experiment [2]. In more concentrated acidic solutions (pH < 6), condensation of molybdate and tungstate occur to form water and isopolymetalates, some of which (e.g., $[M_6O_{21}]^{6-}$, $[M_7O_{24}]^{6-}$) are analogous for the two metals. Protonation constants of $[HM_7O_{24}]^{5-}$ ($\log K_1$ = 4.6 (Mo), 4.8 (W)) are nearly the same [134], as is the case for $[HMO_4]^{1-}$. Condensation reactions involving p equiv. of $[MO_4]^{2-}$ and q equiv. of H^+ are described by the equilibrium constants $\beta_{p,q}$. Values for heptanuclear $[M_7O_{24}]^{6-}$ ($\log \beta_{7,8}$ = 53 (Mo), 65 (W)) and $[HM_7O_{24}]^{5-}$ ($\log \beta_{7,9}$ = 57 (Mo), 69 (W) reveal a greater tendency of W^{VI} toward condensation than Mo^{VI} [134]. A distinguishing feature of condensation reactions is that equilibration in Mo^{VI} systems may be complete in minutes whereas much longer times are often required for W^{VI}. This behavior is an indication of decreased substitutional lability and stronger W^{VI}–O bonds relative to molybdenum.

Because oxidation states below 6+ do not generally sustain more than one M=O bond per M atom in stable species, the

Table 6
Comparative kinetics data for ligand substitution and electron transfer in aqueous solution.

System	k_{298} (s^{-1})	k_{298} ($M^{-1}\ s^{-1}$)	k_{Mo}/k_W	Refs.
$[M_3O_2(OAc)_6(OH_2)_9]^{4+}/H_2O$				
M = Mo	5.6×10^{-6} [a]			
M = W	1.0×10^{-6} [b]		42	[153]
$[M_2O_4(edta)]^{2-}/H_2O$				
M = Mo	6.9×10^{-3}			
M = W	1.16×10^{-4}		59	[156]
$[M_2O_4(OH_2)_6]^{2+}/SCN^-$				
M = Mo		29×10^3 [c]		[157]
M = W		2.5×10^3 [c]	12	[141]
$[M_3O_4(OH_2)_9]^{4+}/SCN^-$				
M = Mo		13.5[d]		[158]
M = W		1.2[d]	11	[159]
$[Mo_2O_4(OH_2)_6]^{2+}/[IrCl_6]^{2-}$				
M = Mo		0.114		[160]
M = W		6.6×10^4	1.7×10^{-6}	[161]
$[M_2O_4(edta)]^{2-}/[IrCl_6]^{2-}$				
M = Mo		6.6[c]		[162]
M = W		6.3×10^5 [c]	1.0×10^{-5}	[156]
$[M_3O_4(OH_2)_9]^{4+}/[IrCl_6]^{2-}$				
M = Mo		4.5		[163]
M = W		1.1×10^6	4.1×10^{-6}	[159]

[a] 323 K; $\Delta H^{\ddagger}$ = 30 kcal/mol; $\Delta S^{\ddagger}$ = 18 eu.
[b] 326 K; $\Delta H^{\ddagger}$ = 14 kcal/mol; $\Delta S^{\ddagger}$ = −39 eu.
[c] Activation parameters determined.
[d] Conjugate base ($[M_3O_4(OH)(OH_2)_8]^{3+}$ reaction pathway.

behavior of these states in aqueous solution is different. The complexes $[Mo^{II}_2(OH_2)_8]^{4+}$ (**7**, red), $[Mo^{III}(OH_2)_6]^{3+}$ (greenish yellow), $[Mo^{III}_2(OH)_2(OH_2)_8]^{4+}$ (**8**, green), $[Mo^{IV}_3O_4(OH_2)_9]^{4+}$ (**9a**, red), and $[Mo^{V}_2O_4(OH_2)_6]^{2+}$ (**10**, yellow) have been identified [138,139]. Aqua ions of lower valent tungsten have proven more difficult to prepare, but the tungsten analogues $[W^{IV}_3O_4(OH_2)_9]^{4+}$ (**9a**, orange) [140] and $[W^{V}_2O_4(OH_2)_6]^{2+}$ (**10**, yellow) [141] have been demonstrated. The complex $[W^{III}(OH_2)_6]^{3+}$ has never been authenticated, possibly because it is too strong a reductant to exist in aqueous media. We note also the remarkable metal sulfidoaqua ions – cuboidal $[M_3S_4(OH_2)_9]^{4+}$ (**9b**), cubane $[M_4S_4(OH_2)_{12}]^{5+}$ (**11**), and corner-shared double cubane $[Mo_7S_8(OH_2)_{18}]^{8+}$ – investigated by Sykes and coworkers [142–144]. Core structures of **7**–**12** are set out in Fig. 6. All of these species are precursors for other polynuclear complexes by ligand substitution. While charges are specified for **9**, **11**, and **12**, these clusters can exist in several oxidation states with retention of core structure and for **11** with different populations of metal atoms in the series $[Mo_{4-n}W_nS_4(OH_2)_{12}]^{z+}$. As a dramatic illustration of metal dependence of potentials, $E_{n=0} - E_{n=4}$ = 825 mV and *ca.* 840 mV for the 6+/5+ and 5+/4+ couples, respectively, in the series [144].

3.2. Reactivity

The most widely studied reaction of molybdenum and tungsten compounds in physiological oxidation states is oxygen atom transfer, which for dithiolene complexes is examined in Section 4.2. The most extensive examples of other types of comparative reactivity are found with low-valent organometallic compounds, frequently carbonyls. While this subject lies outside the purview of this account, we note certain results that are part of a broader trend. In the reversible substitution of $[M(CNBu^t)_7]^{2+}$ with bromide [145], displacement of cycloheptatriene in $[(C_7H_8)M(CO)_3]$ by $P(OMe)_3$ [146], removal of tropylium from $[(C_7H_7)M(CO)_3]^{1+}$ by acetonitrile [147], substitution of $[M(CO)_6]$ with bromide [148] and substitution of CO or bipyridyl in $[M(CO)_4(bpy)]$ by phosphites [149], the kinetics data indicate $k_{Mo} > k_W$ for dissociative and associative pathways. In certain other instances, where the reaction proceeds by nucleophilic attack at a carbonyl carbon rather than directly at the metal atom, as in the system $[M(CO)_6]/Me_3NO$[150], the rate order is W > Mo.

Quantitative data for assessing relative reactivity in physiological oxidation states are limited; representative results for ligand substitution and redox reactions are summarized in Table 6. Rate constants for exchange of bound and solvent water molecules are the widespread measure of intrinsic labilities of metal ions [151,152]. The results for the $M^{IV}_3O_2$ and $M^{V}_2O_4$ (**10**) complexes place them in between $[Ru(OH_2)_6]^{2+}$ ($1.8 \times 10^{-2}\ s^{-1}$) and $[Cr(OH_2)_6]^{3+}$ ($2.4 \times 10^{-6}\ s^{-1}$) or $[Ru(OH_2)_6]^{2+}$ ($3.5 \times 10^{-6}\ s^{-1}$). The positive entropy of activation for the molybdenum complex is indicative of a dissociative mechanism and the negative values for the tungsten complex and that for $[W_3O(OAc)_6(OH_2)_3]^{2+}$ ($k_{298} = 5.3 \times 10^{-4}\ s^{-1}$, $\Delta S^{\ddagger}$ = −31 eu) [153] are consistent with an associative pathway. Rate constants for thiocyanate substitution (in which the product is N-bonded) are much larger due in part to ligand charge but follow the same order. Activation entropies for the M_2O_4 reactions are nearly zero and thus are not mechanistically informative. The water ligands replaced in these reactions are those trans to M=O bonds owing to the trans-labilizing effect of multiply bound oxo ligands. Rate constants for water and thiocyanate substitution show only modest discrimination between metals, the ratio k_{Mo}/k_W being *ca.* 60 or less.

Oxidation reactions of binuclear reactants with $[IrCl_6]^{2-}$ refer to the first step, $M^{V}_2 + Ir^{IV} \rightarrow M^{V}M^{VI} + Ir^{III}$, in the overall reaction. For the $[M_2O_4(edta)]^{2-}$ systems, the rate constant for water substitution is orders of magnitude smaller than the oxidation rate constant, consistent with outer sphere electron transfer. The same is true for the other tungsten complexes. Given the substitution-inert nature of $[IrCl_6]^{2-}$, it is probable that all reactions in Table 6 are outer-sphere processes. The rate order $k_W \gg k_{Mo}$ clearly demonstates that the tungsten complex of a given pair is the more powerful reductant of a constant electron acceptor.

Certain non-quantitative observations also bear on the relative reactivities of molybdenum and tungsten. Among non-redox reac-

tions, when $[Mo_2Cl_9]^{3-}$ is refluxed with pyridine, the product is *mer*-$[MoCl_3(py)_3]$ [154]. In contrast $[W_2Cl_9]^{3-}$ affords $[W_2Cl_6(py)_4]$ after only 2.5 h in refluxing pyridine [155]. The results are indicative of a stronger metal–metal bond in $[W_2Cl_9]^{3-}$. The reversible pH-dependent interconversion between $[M^{IV}(SPh)_2(mnt)_2]^{2-}$ and $[M^{IV}{}_2(SPh)_2(mnt)_4]^{2-}$ is about twice as fast with tungsten than molybdenum [164]. In redox processes, reaction of $[MoS_4]^{2-}$ with sulfur affords $[Mo^{IV}S(S_4)_2]^{2-}$ [165] while under similar conditions $[WS_4]^{2-}$gives $[W^V{}_2(S)_2(\mu_2\text{-}S)_2(S_4)_2]^{2-}$ [166]. Reaction of $[MS_4]^{2-}$ with the disulfides $R_2NC(S)SS(S)CNR_2$ leads to $[Mo^V(S_2)(S_2CNR_2)_3]$ or $[W^{VI}S(S_2)(S_2CNR_2)_2]$ [167]. Further, $[MS_4]^{2-}$ and the disulfide PhC(S)SS(S)CPh produce $[Mo^{IV}(S_2CPh)_4]$ or $[W^{VI}S(S_2)(S_2CPh)_2]$ [168]. In cases where the metal is reduced below M^{VI}, the reaction is one of induced internal electron transfer. The metal is reduced in the presence of sulfur or disulfide. Bound sulfide is the reductant, in some cases being oxidized to persulfide. Exact reaction stoichiometries have not been established in most cases and the outcome of some reactions depends on conditions and reactants. For example, both complexes $[M^V{}_2(S)_2(\mu_2\text{-}S)_2(S_4)_2]^{2-}$ can be obtained from $[MS_4]^{2-}$ and sulfur in DMF at ~100 °C under anaerobic conditions [166]. However, a trend emerges. Tungsten systems sustain ligand redox and the metal, if affected, is not reduced below W^V whereas in molybdenum systems the metal is reduced to $Mo^{IV,V}$ with accompanying ligand redox. This result is consistent with the relative oxidative stabilities of molybdenum and tungsten (Section 2.5).

With recognition of a limited database of results, the following summary of principal reactivity features for $M^{IV,V}$ complexes is offered.

- *Rate constants for ligand substitution and electron transfer follow the order $k_{Mo}/k_W \lesssim 60$ and $k_W/k_{Mo} \approx 10^5$–10^6, respectively, in aqueous solution at 25 °C.*

4. Dithiolene complexes as synthetic analogues of catalytic sites

All molybdenum- and tungsten-containing enzymes utilize mononuclear catalytic sites in which one or two pyranopterindithiolate cofactor ligands **1** (Fig. 2) are chelated to a metal atom in oxidation states $M^{IV–VI}$. The ligand is depicted as an ene-1,2-dithiolate, the most reduced form of an extensive family of redox-active dithiolene ligands. As noted earlier and considered subsequently (Section 5.3), this form applies to synthetic analogues and catalytic sites in each metal oxidation state. Dithiolene ligands are of two fundamental types (Fig. 2), the ene-1,2-dithiolenes $R_2C_2S_2$ and benzene-1,2-dithiolenes $C_6H_{4-n}X_nS_2$ with widely variable R and X substituents, whose most prominent property is modulation of redox potentials. Nearly all important contemporary aspects of metal dithiolenes have been covered in the volume "Dithiolene Chemistry" [169] including their synthesis [170]. An account of the early development of metal dithiolene chemistry starting in 1962 is available [171]. In the following section, synthetic methods affording primarily site analogues containing one or two dithiolene ligands are summarized. Inasmuch as protein sites with three cofactor ligands are unknown, the synthesis of tris(dithiolenes) is excluded. However, references to their preparation as well to mono- and bis-dithiolene complexes are provided in Table 2.

4.1. Synthesis

Dithiolene ligands play a significant role in the development of structural and functional synthetic analogues because they simulate the structural and electronic features in the immediate coordination environment of molybdenum and tungsten when chelated by the cofactor ligand **1**. Frequently employed dithiolenes for this purpose include mnt, bdt, and mdt (Fig. 2). The first two are available as isolated salts. The mdt ligand, which has not been isolated as such, was selected for use in the Harvard laboratory because it carries alkyl substituents similar to the carbon centers proximal to the dithiolene portion of **1**. More recently, improved preparations using 4,5-dimethyl-1,3-dithiol-2-one as a precursor to mdt complexes have been reported [64], and precursors of the ligands $S_2C_5H_6X$ have been prepared, allowing access to a broader range of alkyl-substituted complexes [172]. A DFT analysis of the ligand modeling problem has led to the suggestion that a dithiolene functionality as part of a pyran ring to which is fused a pyrazine ring would be preferable to the aforementioned dithiolenes [173], but no such ligand has yet been prepared. Consideration of the structural and electronic interplay between a dithiolene grouping and the remainder of **1**, including possible facilitation of electron transfer to or from the metal site that accompanies atom transfer [174], emphasizes the attractiveness of a ligand of this type.

4.1.1. Bis(dithiolene) complexes

Reactions affording bis(dithiolene)$M^{IV–VI}$ complexes are set out in Fig. 7. A particularly useful procedure is carbonyl displacement from the dicarbonyl **13**, prepared by ligand transfer from $[Ni(S_2C_2R_2)_2]$ to $[M(CO)_3(MeCN)_3]$ [37,62,61]. In this way, an array of five-coordinate square pyramidal M^{IV} complexes **14**–**18** are readily accessible [38,52,53,56,37,172]. Further reactions afford the M^V=O complexes **19** [62], the $W^{VI}O_2$ complex **20**, and the W^{VI}=Q species **21** and **22** (Q = O, S) [38,56]. Other reactions of interest include ligand substitution of isonitrile complex **23** to yield **24** or **25** [43], dithiolene ring formation from bis(tetrasulfido) **26** and an alkyne to give **25** [47,175], oxidation of **24** with the strong oxo donor Me_3NO to yield **27** [28,68,71], and silylation of a terminal oxo ligand to form silyloxide complexes **28** [42,43,59]. These reactions were carried out in aprotic solvents, typically acetonitrile. Mnt complexes **29** can be prepared from $[MO_4]^{2-}$ in aqueous solution, the Mo^{IV} complex being formed with the mild reductant bisulfite [28,176]. The W^{IV} complex requires the strong reductant dithionite [30], in keeping with the relative reducibilities of the M^{VI} state. Protonation of **29** in the presence of Ph_3P and other ligands affords the six-coordinate Mo^{IV} complexes **30** [177–179]. Similar M^{IV} complexes of the general types $[M(S_2C_2R_2)_2L_2]$ (L = RNC, PR_3) [43,59,64] and $[M(S_2C_2R_2)_2(CO)L]^z$ (L = PR_3, RS^-, RSe^-) [56,37,64], some of which approach trigonal prismatic stereochemistry, have been prepared. Reaction of aqueous $[MO_4]^{2-}$ at pH 5.5–6 with Na_2(mnt) yields the $M^{VI}O_2$ complexes **31**, analogous to **27**. Tungsten complex **31** with sulfur forms the dianionic persulfide **32** [30]. Related complex **33** forms the persulfide species **34** [180], which can be reduced with dihydrogen to **33** [181].

Fig. 7 is intended as a summary of the most useful methods for the synthesis of bis(dithiolene) complexes. It is not comprehensive; however, most omitted reactions are extensions or variations of those shown. One interesting exception is the synthesis of $[MO(tfd)_2]^{2-}$ from $[MoO_2S_2]^{2-}$ or $[WOS_3]^{2-}$ and the dithiete $(CF_3)_2C_2S_2$ by means of induced internal electron transfer in which the oxidized metal and dithiete are reduced by two electrons and sulfido ligands are oxidized [36]. This is in contrast to the reactions affording $[M(tfd)_3]$ in which the reduced metal supplies electrons for reduction of the dithiete [78]. Five-coordinate complexes from the foregoing methods are square pyramidal with the metal situated *ca.* 0.7 A above the S_4 basal plane. Monooxo and dioxo M^{VI} complexes assume a highly distorted octahedral structure with an oxo ligand cis to a non-dithiolene ligand. Certain of the reactions, such as **14** → **20**, **18** → **22**, and **24** → **27**, are oxygen atom transfer processes. These complexes are site analogues in functional reaction systems related under the Hille classification to the DMSOR enzyme family [6]. Here and elsewhere RO^-, RS^-, and RSe^- ligands

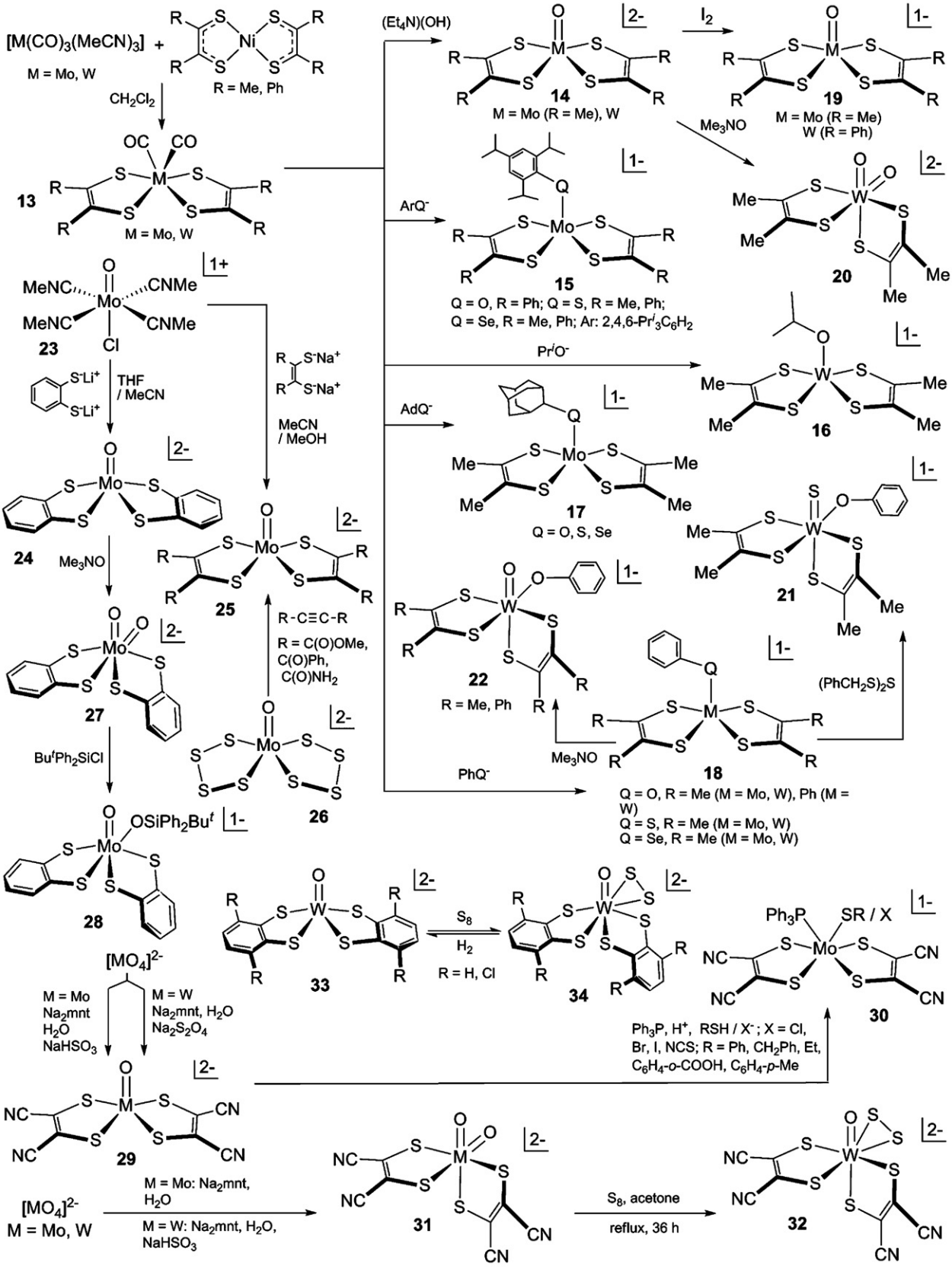

Fig. 7. Synthesis of selected bis(dithiolene) M^{IV-VI} complexes as synthetic analogues of enzyme sites.

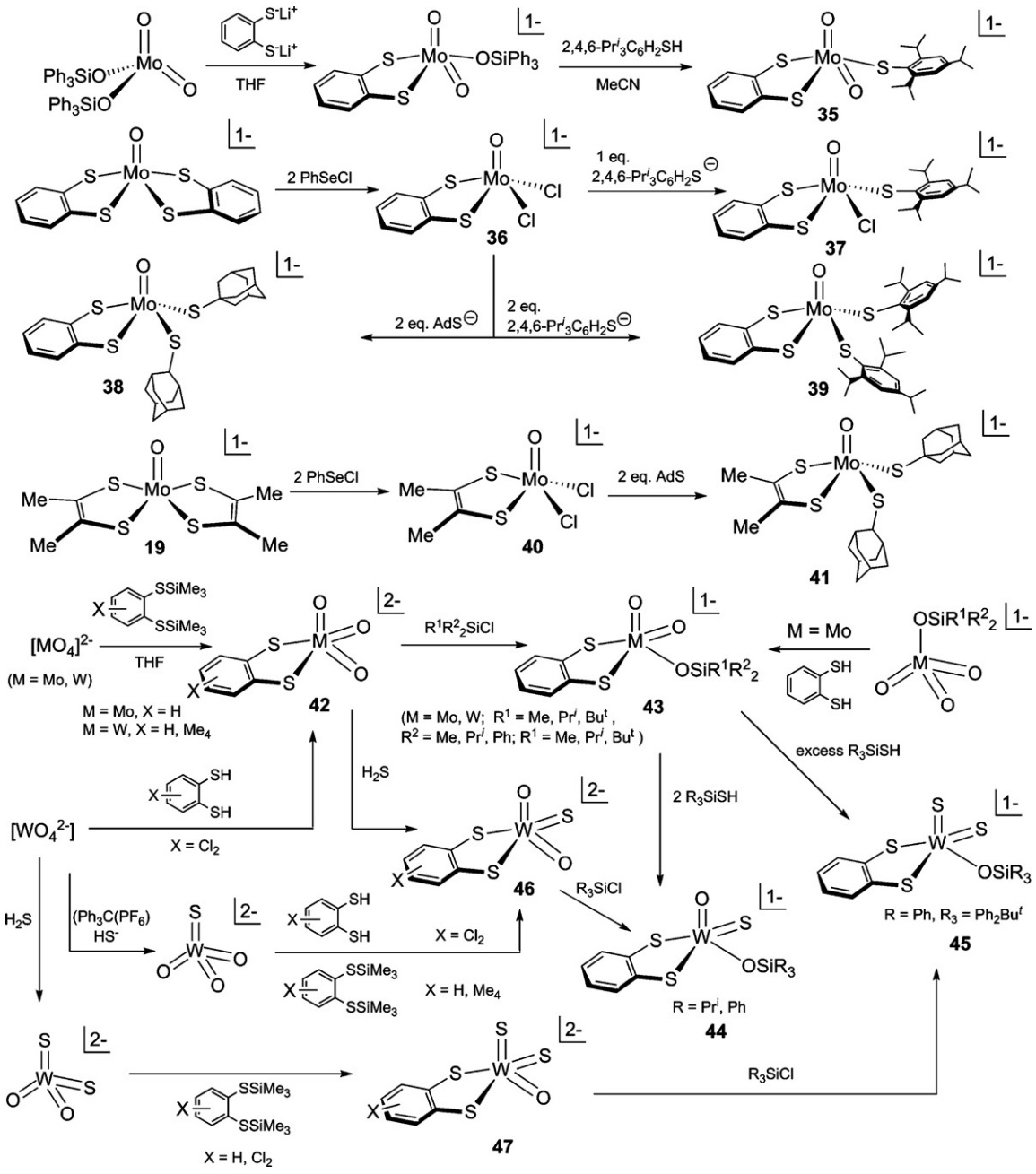

Fig. 8. Synthesis of mono(dithiolene) $M^{V,VI}$ complexes.

impersonate native binding by serinate, cysteinate, and selenocysteinate, respectively.

4.1.2. Monodithiolene complexes

This class is much less populated than the bis(dithiolenes), due in part to the lack of general preparative methods. Synthesis has been pursued mainly by the Harvard laboratory [23–26]; selected reactions are summarized in Fig. 8. Monothiolate $Mo^{VI}O_2$ complex **35** is obtained by substitution reactions with formation of Ph_3SiOLi and Ph_3SiOH in successive steps. The key step in the formation of $Mo^{V}O$ complex **37** is the bis(dithiolene) to monodithiolene conversion effected by removal of one bdt ligand as $C_6H_4(SSePh)_2$ upon reaction with the electrophile PhSeCl. The product **36** is subject to chloride substitution by thiolate, leading to **38** and **39**. A similar reaction sequence starting with **19** affords **40** and **41** [25]. Treatment of $[MO_4]^{2-}$ with $C_6H_4(SSiMe_3)_2$ affords the valuable $M^{VI}O_3$ complexes **42** and $(Me_3Si)_2O$ [23]. These complexes can be monosilylated to afford an extensive set of products which with M = W sustains mono- and disulfidation reactions with silylthiols leading to **44** and **45**, respectively [24,26]. Controlled reaction of tungsten complex **42** with H_2S or the indicated reactions based on $[WO_3S]^{2-}$ afford monosulfido **46** while disulfido **47** is accessible from $[WO_2S_2]^{2-}$ and $C_6H_4(SSiMe_3)_2$. Reactions utilizing silylsulfur reagents benefit from the contributory enthalpic driving force owing to the *ca.* 30–40 kcal/mol difference between Si–O and Si–S bond energies [23].

Monodithiolene complexes are sought as potential analogues of the active sites in the XOR enzyme family [6]. The majority of complexes in Fig. 8 are essentially square pyramidal with an apical oxo ligand, as are the native sites. Some variability in structures between the square pyramidal and trigonal bipyramidal limits has been observed for $[MO_{3-n}S_n(bdt)]^{2-}$ species. The calculated

Table 7
Comparative kinetics data for pairs of M^{IV} and M^{VI} complexes in oxo transfer reactions at 298 K.

Reactant	Substrate	k_2 or k_2' (M^{-1} s^{-1})[a]	ΔH (kcal/mol)	ΔS (eu)	k_2^W/k_2^{Mo} [d]	Refs.
$[MO_2(mnt)_2]^{2-}$						
M = Mo	$(MeO)_2PhP$	4.5×10^{-1}	8.2	−33		[4]
M = W		4.5×10^{-4}	11	−38	1.0×10^{-3}	
M = Mo	$(MeO)_3P$	2.5×10^{-2}	10	−32		
M = W		9.7×10^{-6}	14	−33	3.9×10^{-4}	
M = Mo	$(EtO)_2MeP$	1.1	–	–		
M = W		3.4×10^{-3}	–	–	3.1×10^{-3}	
$[MO(bdt)_2]^{2-}$						
M = Mo	Me_3NO	2.0×10^{-4} [b]	–	–		[71]
M = W		5.0×10^{-3} [b]	–	–	25[b]	
$[M(OPh)(mdt)_2]^{1-}$						
M = Mo	Me_2SO	1.3×10^{-6}	14.8	−36		[52]
M = W		3.9×10^{-5}	14.4	−30	30	[53]
M = Mo	$(CH_2)_4SO$	1.5×10^{-4}	10.1	−39		[52]
M = W		9.0×10^{-4}	11.6	−33	6.0	[53]
M = Mo	Ph_3AsO	2.8×10^{-2}	7.2	−39		
M = W		3.1	9.3	−26	111	[57]
M = Mo	SeO_4^{2-}	7.2×10^{-4}	12	−34		
M = W		3.3×10^{-3}	12.8	−28	4.6	[51]
$[M(OC_6H_4\text{-}p\text{-}OMe)(mdt)_2]^{1-}$ [c]						
M = Mo	Ph_3AsO	2.4×10^{-2}	7.3	−40		
M = W		1.9	98	−25	79	[57]
$[M(OPh)(mdt)_2]^{1-}$						
M = Mo	$(CH_2)_4SO$	3.4×10^{-4}	–	–		[52]
M = W		3.0×10^{-3}	9.0	−40	8.8	[192]

[a] Acetonitrile or DMF solutions.
[b] k_{obs} and ratio of k_{obs} values.
[c] For other reaction systems $[M(OC_6H_4\text{-}p\text{-}X)(mdt)_2]^{1-}/Ph_3AsO$, k_2^W/k_2^{Mo} 184 (X = Br) and 163 (X = COMe).
[d] Ratio of k_2 or k_2'.

energy differences between these structures for a given *n* are a few kcal/mol with the square pyramidal arrangement favored, suggesting that solid state interactions are responsible for irregular conformations [24]. Complex **35** is an analogue of the oxidized site $[Mo^{VI}O_2(S_2pd)(S_{Cys})]$ in chicken liver sulfite oxidase. Square pyramidal **46**, having the long-sought $M^{VI}O_2S$ group with the sulfido ligand in the basal plane, serves as structural analogue of the unprotonated site in enzymes such as quinoline-2-oxidoreductase and bovine milk XOR (Fig. 3). The complex is not a chemical model because the native metal in this enzyme family is molybdenum. The corresponding molybdenum complex has not been isolated, apparently because of autoredox instability also observed in other cases with Mo^{VI} in an anionic sulfur (reducing) environment. However, given the generalization in Section 2.3, W^{VI} is an accurate structural surrogate of Mo^{VI}. As yet, no functional reaction systems using monodithiolene complexes have been developed for any member of the XOR enzyme family.

4.2. Oxo transfer reactions and kinetics

The first comprehensive treatment of metal-centered oxygen atom (oxo) transfer reactions appeared in 1987 [182] followed in 1990 [183] by a description of molybdenum-mediated reactions in synthetic systems and their relation to some aspects of enzyme catalysis. Thereafter, a multitude of articles on oxomolybdenum complexes and their role in oxo transfer systems have appeared, no doubt stimulated in large part by advances in understanding enzymatic reactions. In addition to previous citations [14–17], we note three earlier summary articles on the biomimetic chemistry of molybdenum and tungsten [48,184,185] and one dealing with the model chemistry of Mo-mnt systems [186]. Thoroughout this period, the imperative of biomimetic tungsten chemistry has been slowly growing, but understandably has lagged far behind that of molybdenum because of the larger number of molybdenum oxotransferases and hydroxylases of known function that have been purified and structurally defined. In this section, the principal issues are analogue reaction systems and the comparative kinetics of pairs of molybdenum and tungsten reactants with constant substrate.

4.2.1. Basic features

Oxo transfer reactions may be minimally described as below and, if second-order, with the indicated rate laws for the forward and reverse reactions. The forward reaction is oxo transfer from substrate and the reverse oxo transfer to substrate with concomitant metal oxidation and reduction, respectively. Associative transition states are

$$M^{IV} + XO \rightleftarrows M^{VI}O + X \qquad -d[M^{IV}]/dt = k_2[M^{IV}][XO]$$

$$-d[M^{VI}O]/dt = k_2'[MO^{VI}][X]$$

consistent with large negative entropies of activation. Kinetics data for the reverse reaction, in which P^{III} compounds are oxidized to P^VO products, are found in Table 7. Rate constants at constant substrate show the order $k_2'^{Mo} > k_2'^{W}$ with $\Delta S^{\ddagger} = -32$ to -38 eu.

4.2.2. Analogue reaction systems

In this section, we describe dithiolene-based analogue reaction systems capable of executing stoichiometric reactions with biological substrates using in most cases chemical apparatus (analogues) credibly resembling native enzyme sites, all of which are found in the DMSOR family [6]. These systems are schematically depicted in Fig. 9 in which variable substituents are designated R,R^1,R^2. All available comparative kinetics data for molybdenum and tungsten systems are collected in Table 7. Other data compilations are available elsewhere [14,51,57].

- *DMSO and TMNO reduction:*

$$Me_2SO + 2H^+ + 2e^- \rightleftarrows Me_2S + H_2O$$

$$Me_3NO + 2H^+ + 2e^- \rightleftarrows Me_3N + H_2O$$

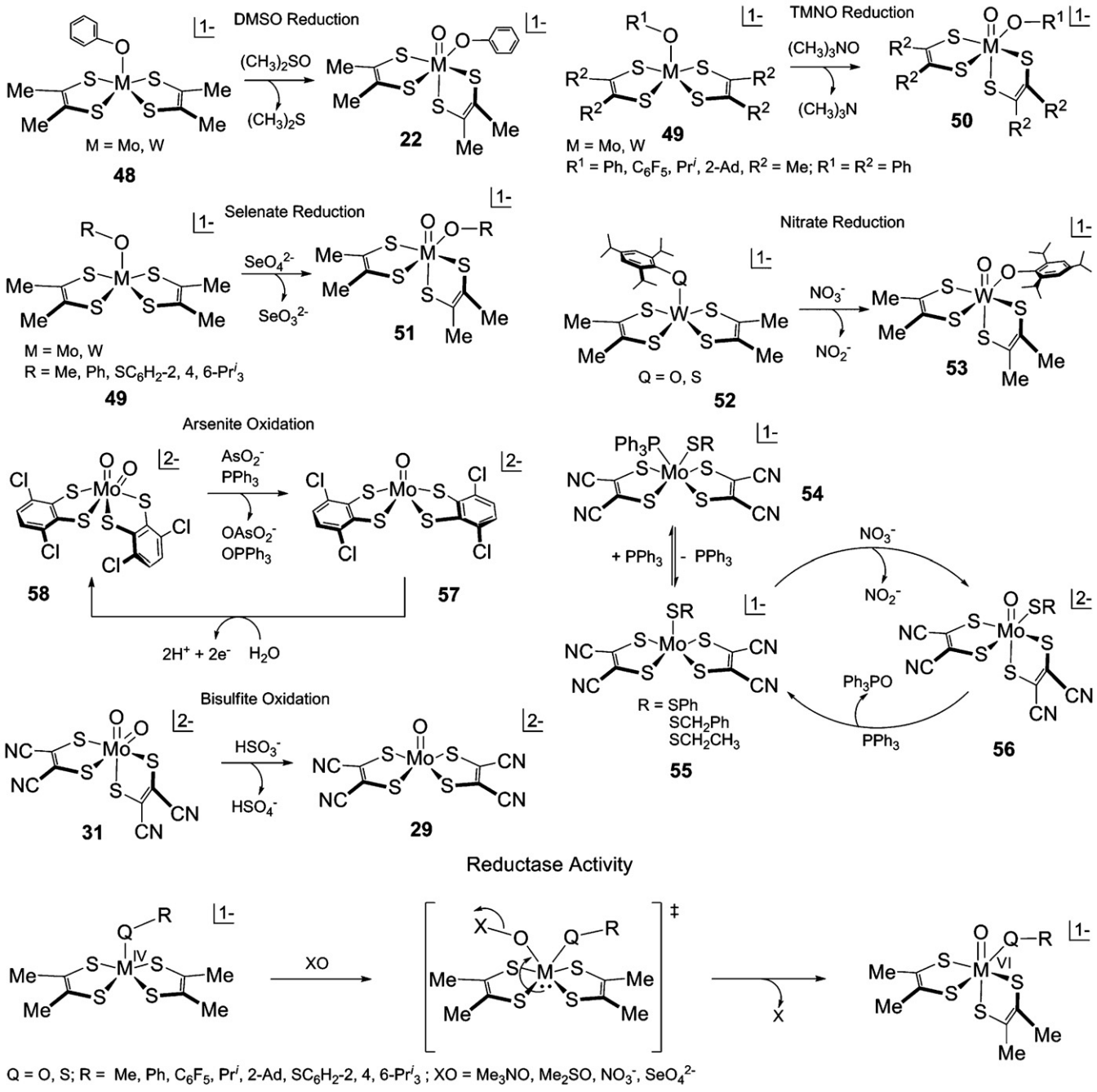

Fig. 9. Schematic descriptions of analogue reaction systems and depiction of the substrate reduction pathway.

reduced enzyme site [187–191]: $[Mo^{IV}(O_{Ser})(S_2pd)_2]$

analogue reactions [29,42,52,53,55,59,192]:

$$[M^{IV}(OR')(S_2C_2R_2)_2]^{1-} + R''_2SO/R''_3NO \rightarrow [M^{VI}O(OR')(S_2C_2R_2)_2]^{1-} + R''_2S/R''_3N$$

These reactions proceed readily with illustrative rate constants k_2 for the reaction **48** → **22** in the 10^{-5}–$10^{-6}\,M^{-1}\,s^{-1}$ range and large negative entropies of activation (Table 7) indicative of associative transition states. The rate constants with *N*-oxides are larger than with *S*-oxides, as in the conversion **49** → **50** with M = Mo ($k_2 = 200\,M^{-1}\,s^{-1}$) and $\Delta S = -21$ eu [52]. One complication in reactions with $[Mo(OR')(S_2C_2Me_2)_2]^{1-}$ is the instability of the Mo^{VI} product due to autoredox, leading to the isolation of $[Mo^{V}O(mdt)_2]^{1-}$ [52]. All $W^{VI}O$ complexes such as **22** and **50** are isolable and their structures have been established. Recently, it has been demonstrated that the reaction product of $[Mo(OSiR_3)(S_2C_2(CO_2Me)_2)_2]^{1-}$ and Me_3NO is $[MoO(OSiR_3)(S_2C_2(CO_2Me)_2)_2]^{1-}$ [193]. This complex can be isolated, is essentially isostructural with related tungsten complexes, and has an absorption spectrum similar to oxidized DMSOR, marking it as an oxidized site analogue. It is foreshadowed by isostructural **28** which, however, was prepared by silylation of $[MoO_2(bdt)_2]^{2-}$ rather than by oxo transfer [43]. The less electron-rich nature of the dithiolenes and steric protection offered by the large silyloxide ligands contribute to the stability of these $Mo^{VI}O$ complexes.

Oxo transfer with *N*-oxides is a standard preparative method, as exemplified by the conversions in Fig. 7. One of these, $[MoO(R_2bdt)_2]^{2-} \rightarrow [MoO_2(R_2bdt)_2]^{2-}$, while not related to a bio-

logical reaction, is among the first oxo transfer reactions not complicated by the formation of a non-physiological Mo^{V}–O–Mo^{V} species [40]. The rate of reaction was found to be *ca.* 25 times slower than that of $[WO(bdt)_2]^{2-}$ with the same substrate, a rate order than extends to other systems (Table 7).

- *Selenate reduction*:

$$SeO_4^{2-} + 2H^+ + 2e^- \rightleftarrows SeO_3^{2-} + H_2O$$

reduced enzyme site [194]: $[Mo^{IV}(OH)(S_2pd)_2]$
analogue reactions [51]:

$$[M^{IV}(OR)(S_2C_2Me_2)_2]^{1-} + SeO_4^{2-} \rightarrow [M^{VI}O(OR)(S_2C_2Me_2)_2]^{1-} + SeO_3^{2-}$$

These reactions, depicted as **49** → **51** in Fig. 9, proceed with M = Mo and W and R = Ph or Me with $k_2 \approx 10^{-3}$–10^{-4} M^{-1} s^{-1}, large negative activation enthalpies, and slightly faster rates with tungsten (Table 7). Selenate consumption and selenite formation were directly observed by ^{77}Se NMR.

- *Nitrate reduction (dissimilatory):*

$$NO_3^- + 2H^+ + 2e^- \rightleftarrows NO_2^- + H_2O$$

reduced enzyme site [195,196]: $[Mo^{IV}(S_{Cys})(S_2pd)_2]$
analogue reactions [58,177,178]:

$$[W^{IV}(QR)(mdt)_2]^{1-} + NO_3^- \rightarrow [W^{VI}O(QR)(S_2C_2Me_2)_2]^{1-} + NO_2^- \quad (i)$$

$$[M^{IV}(SR)(mnt)_2]^{1-} + NO_3^- \rightarrow [M^{VI}O(SR)(mnt)_2]^{1-} + NO_2^- \quad (ii)$$

Two reaction systems have been developed in relation to the cysteinate-ligated native site. In system (i), tungsten complexes **52** with sterically hindered axial ligands support nitrate reduction in second-order reactions with $k_2 = 0.17\ M^{-1}\ s^{-1}$ (Q = S) and $6.1 \times 10^{-3}\ M^{-1}\ s^{-1}$ (Q = O); the corresponding molybdenum complexes were not well-behaved [58]. Product **53** (Q = O) was verified by independent synthesis. In system (ii) in dichloromethane, reversible dissociation of phosphine from **54** produces **55** which reacts with nitrate to afford nitrite and **56**. The system follows Michaelis–Menten saturation kinetics which with *R* = *Et* gives $V_{max} = 3.2 \times 10^{-2}\ s^{-1}$. $Mo^{VI}O$ complex **56** can be reduced back to **55**, establishing a catalytic cycle, but could not be isolated owing to its nitrosylation by nitrite to yield $[Mo(NO)_2(mnt)_2]^{2-}$ [177,178].

- *Arsenite oxidation:*

$$H_2AsO_3^-(AsO_2^-) + H_2O \rightleftarrows HAsO_4^{2-}(AsO_3^-) + 3H^+ + 2e^-$$

reduced enzyme site [197,198] $[Mo^{IV}(S_2pd)_2]$
analogue reaction [199]:

$$[Mo^{VI}O_2(Cl_2bdt)_2]^{2-} + AsO_2^- \rightarrow [Mo^{IV}O(Cl_2bdt)_2]^{2-} + AsO_3^-$$

Electrochemical oxidation of **57** in acetonitrile/water or chemical oxidation in the presence of hydroxide affords $Mo^{VI}O_2$ complex **58** (a variant of **27**). The latter is reported to stoichiometrically oxidize arsenite to arsenate and also Ph_3P to Ph_3PO [199].

Four of the foregoing five systems result in substrate reduction, which lends itself to the summary depiction in Fig. 9. Here an associative transition state is produced by M···OX intereaction and likely M–QR bond loosening. Transfer of two electrons to the interacting substrate to develop the M=O bond with X–O bond scission, dissociation of the reduced product X, and structural reorientation to the final cis stereochemistry complete the process. Reversal of these events results in substrate reduction. The mechanism of substrate reduction is examined in greater detail with spectroscopic data and theoretical calculations in Section 5.3.

Lastly, we note certain other reactivities which, while not necessarily analogue reactions themselves, are worthy of extension and further study. The bisulfite reaction system, in which **31** is reduced to **29** in acetonitrile/water (Fig. 9) [200], is not an analogue reaction system because of the presence of two dithiolene ligands but it is the cleanest oxo transfer demonstration of sulfite oxidation mediated by molybdenum. The reaction follows Michaelis–Menten kinetics with $K_M = 0.001$ M and $k_2 = 0.87\ s^{-1}$. A subsequent investigation confirmed the kinetics scheme but with different parameters ($K_M = 0.039$ M, $k_2 = 1.02\ s^{-1}$) [69]. Several interesting transformations based on $[WO(mnt)_2]^{2-}$ have been reported. In acetonitrile-water, bicarbonate forms $[WO_2(mnt)_2]^{2-}$ (**31**) and formate in a reaction related to tungsten formate dehydrogenase [35]. The complex is also described as a catalyst for the non-redox hydration of acetylene to acetaldehyde, a reaction catalyzed by acetylene hydratase [201]. Lastly, $[WO(S_2)(mnt)_2]^{2-}$ (**32**) was found capable of mediating the transformation of an aldehyde (crotonaldehyde) to a carboxylic acid (crotonic acid) [30], a model reaction for aldehyde ferredoxin oxidoreductase.

The following conclusions derive from the foregoing results.

- *Meaningful analogue reaction systems can be realized that are capable of transforming biological substrates and utilizing as reactants molybdenum and tungsten complexes that are accurate (though not necessarily optimal) structural and electronic analogues of the coordination units in enzyme sites. Such systems resemble single-turnover enzyme reactions and convey mechanistic information.*
- *For second-order substrate transformations, kinetic metal effects – $k_2^{W} > k_2^{Mo}$ for substrate reduction ($M^{IV} \rightarrow M^{VI}$) and $k_2'^{Mo} > k_2'^{W}$ for substrate oxidation ($M^{VI} \rightarrow M^{IV}$) – are consistently operative.*

5. Case studies

5.1. Isoenzymes

Molybdenum and tungsten isoenzymes are encoded by different genes, contain different metals at their catalytic sites, and perform the same reaction. Examples are found with the methanogenic archaea *M. thermoautotrophicum* and *M. wolfei*, each of which contains two separate formylmethanofuran dehydrogenases which catalyze the first step in methane formation from CO_2 [202–204]. There are cases in which tungsten has been successfully substituted for molybdenum although sometimes with a change in pH activity profile. Examples include active enzyme formation by replacement of the native metal molybdenum with tungsten in *R. capsulatus* DMSOR expressed in *E. coli* [205] and in *E. coli* TMNO reductase [206]. Relative reactivities of these and other isoenzymes are found in Table 8. Note that in the FMDH reactions in which the substrate is oxidized and the metal is reduced, and in the TMNOR reactions in which the substrate is reduced and the metal is oxidized, the rate discriminations are rather small but the rate orders are Mo > W and W > Mo, respectively. Mo-DMSORs reduce both DMSO and TMNO and Mo-TMNORs reduce *N*-oxides but not *S*-oxides at a measurable rate [206]. Relying on values of k_{cat}/K_M, the rate order is W > Mo.

By far the most thoroughly examined isoenzymes are the DMSORs from *R. capsulatus* [205,207]. An enzyme strain grown in the presence of 3 μM Na_2WO_4 and a slight concentration of Na_2MoO_4 incorportated tungsten in place of molybdenum, and the tungsten enzyme was found to crystallize under the same conditions as oxidized Mo-DMSOR. A substantial body of crystallographic and spectroscopic data demonstrates that two oxidized enzymes exhibit the same protein fold and environment around the catalytic

Table 8
Relative reactivities of molybdenum and tungsten isoenzymes[a].

Isoenzymes	Organism	Reaction		W/Mo reactivity ratio[b]	Refs.
FMDH	*M. thermoautotrophicum*	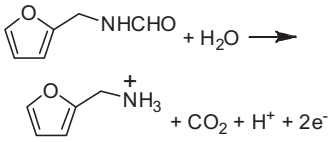		0.2	[204]
					[210]
	M. wolfei			0.3	[208]
			$\frac{XO}{Me_3NO}$	2.2	
			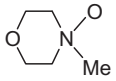	4.1	
				4.2	
				2.0	
TMNOR	*E. coli*	$XO + 2H^+ + 2e^- \rightarrow X + H_2O$	Me_2SO	Mo: no reaction; W: $k_{cat}/K_M = 5.0 \times 10^4\ M^{-1}\ s^{-1}$	[206]
			Ph_2SO	Mo: no reaction; W: $k_{cat}/K_M = 2.7 \times 10^4\ M^{-1}\ s^{-1}$	
				Mo: no reaction; W: $k_{cat}/K_M = 2.0 \times 10^6\ M^{-1}\ s^{-1}$	
DMSOR	*R. capsulatus*	$MeSO_4 + 2H^+ + 2e^- \rightleftharpoons Me_2SO + H_2O$		17 (forward) ≤0.006 (reverse)	[213]

[a] Adapted from Ref. [53].
[b] Ratios of rate constants.

site, and highly similar $[M^{VI}O(O_{Ser})(S_2pd)_2]$ coordination units found in other DMSORs. A principal point at issue is the presence of an additional oxygen atom at a seven-coordinate molybdenum site, as reported in the crystal structure of the oxidized enzyme [208]. X-ray data for oxidized W-DMSOR do not resolve the issue; the active site has been depicted as six-coordinate [205]. Molybdenum EXAFS for the oxidized enzyme from *R. sphaeroides* and an examination of the results for the *R. capsulatus* enzyme by George et al. [188] support a six-coordinate site. These isoenzymes reduce DMSO and oxidize Me_2S according to the foregoing rate orders. Further note that the order W > Mo for the reduction of *N*-oxides and *S*-oxides is that observed in analogue reaction systems (Table 7).

The *R. capsulatus* isoenzymes currently provide the only comparative redox potentials in essentially identical protein environments [209]. While other reported values differ somewhat

E_m = +26 mV ($Mo^{VI/V}$, pH 8), −194 mV ($W^{VI/V}$, pH 7)
E_m = +200 mV ($Mo^{V/IV}$, pH 8), −134 mV ($W^{V/IV}$, pH 7)

[205], in part because the $M^{VI/V}$ step is pH-dependent, it seem reasonable to approximate $E_{Mo} - E_W \approx 200$–300 mV, values roughly comparable to the potential difference of bis(dithiolene) redox couples in aprotic media (Table 5).

On the basis of limited data, the following observation is offered.

- *Intrinsic trends in reaction rates accompanying oxo transfer with substrate oxidation (Mo > W) and reduction (W > Mo) and redox potential orders for $M^{VI/V}$ and $M^{V/IV}$ couples (Mo > W) are expected properties of isoenzymes. Departures from these regularities imply specific protein influence(s) very likely affecting the metal coordination unit directly.*

5.2. Relativistic effects: monooxo bis(dithiolene) complexes $[M^VO(bdt)_2]^{1-}$

In this section, certain properties of the pair $[M^VO(bdt)_2]^{1-}$ [39,41,45] are examined as a means of assessing the influence of relativistic effects in tungsten. These complexes have approximately square pyramidal geometry (C_{4v} symmetry) with a strong axial oxo ligand, and thus, bonding calculations predict that the metal d orbitals split into three groups. At lowest energy is the approximately non-bonding $d_{x^2-y^2}$ orbital (*x*- and *y*-axes bisect the S–M–S angles). Next, the d_{xz}/d_{yz} orbitals have π anti-bonding interactions with the O p_x/p_y and out-of-plane dithiolene S p orbitals. Finally, with the highest energies, are the d_{xy} and d_{z^2} orbitals, which have σ anti-bonding interactions with the in-plane dithiolene S p orbitals and the O p_z orbital, respectively. Since these complexes are in the M^V oxidation state, each has a metal d^1 configuration with the single electron in the redox-active $d_{x^2-y^2}$ orbital.

The ligand K-edge XAS methodology developed by Hedman, Hodgson, and Solomon [211,212] provides a unique opportunity to study the energies of unfilled molecular orbitals of transition metal complexes (of relevance here, the metal $d_{x^2-y^2}$ in $[M^VO(bdt)_2]^{1-}$). The excitation of ligand 1s electrons into the continuum results in an absorption feature known as an edge, while excitations to the unfilled valence molecular orbitals result in "pre-edge" features. The pre-edge peaks often appear at energies lower than the edge. The energies of these pre-edges have three contributions: ligand effective nuclear charge (Z_{eff}), metal Z_{eff}, and the ligand field. Increasing ligand Z_{eff} stabilizes the 1s orbital, thus increasing the energy of the pre-edge feature. In contrast, increasing metal Z_{eff} stabilizes metal-based orbitals which decreases the energy of the pre-edge peak. Finally, a stronger ligand field destabilizes the valence orbitals, and thus, the energy of the pre-

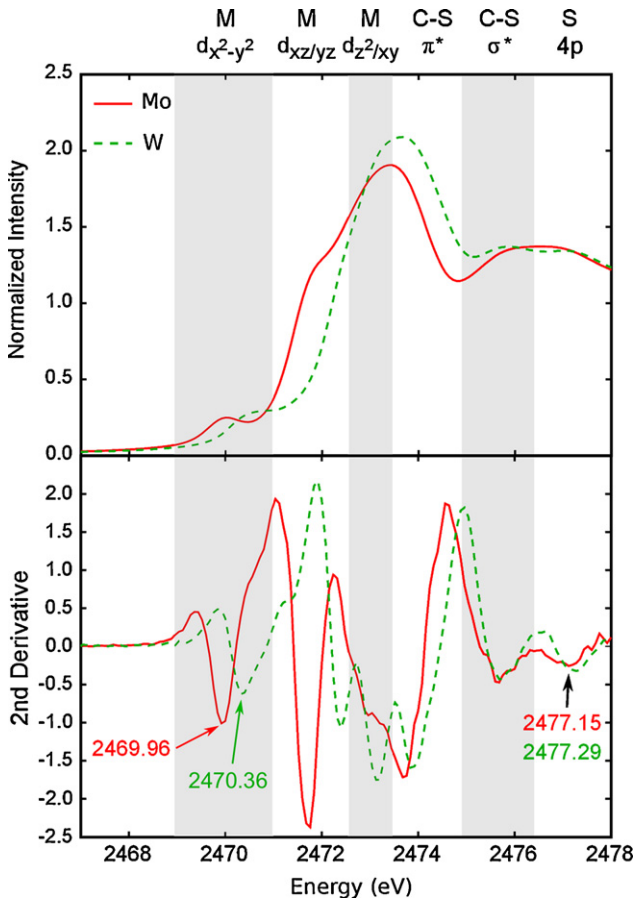

Fig. 10. The sulfur K-edge XAS normalized and second derivative data for $[MO(bdt)_2]^{1-}$ (M = Mo, W). Note that the metal-based pre-edges are shifted higher for W than for Mo while the ligand-based pre-edges are at similar energies.

edge feature increases. Therefore, for similar complexes such as $[MO(bdt)_2]^{1-}$, ligand K pre-edge energies can be used to quantify differences in metal Z_{eff}, and any differences in metal Z_{eff} imply that the valence electrons are shielded differently from the nuclear charge.

The sulfur K-edge XAS normalized and second derivative data for $[M^{V}O(bdt)_2]^{1-}$ are shown in the top and bottom panels of Fig. 10, respectively. Note that minima in the second derivative data can be used as estimates of peak positions. As expected from bonding considerations, the metal-based pre-edge features are divided into three groups dependent upon the strength of the anti-bonding interactions between metal and ligand orbitals. Transitions to the non-bonding M $d_{x^2-y^2}$ orbital result in resolved pre-edge peaks at ~2470 eV, while transitions to π anti-bonding M d_{xz}/d_{yz} orbitals (~2472 eV) and σ anti-bonding M d_{xy}/d_{z^2} orbitals (~2473 eV) result in features that are not fully resolved from the edge but are observed in the second derivative. Pre-edge features that are still higher in energy have been assigned as transitions to dithiolene ligand-based orbitals: C–S π* (~2474 eV), C–S σ* (~2476 eV), and S 4p (~2477 eV) [213]. There are two important observations to make in Fig. 10: (i) transitions to metal-based orbitals are higher in energy in the W data (dotted green) compared to the Mo data (solid red), and (ii) transitions to ligand-based orbitals have similar energies in the spectra of both the Mo and the W complexes. Taken together, these observations indicate that the W d orbitals are destabilized relative to their Mo counterparts and there is little difference in sulfur Z_{eff} between the two complexes. Specifically, the redox-active W $d_{x^2-y^2}$ is 0.26 eV higher in energy than the Mo $d_{x^2-y^2}$ after taking into account differences in sulfur Z_{eff} as determined from transitions to the S 4p orbital (*i.e.* 0.14 eV from the second derivative data in Fig. 10).

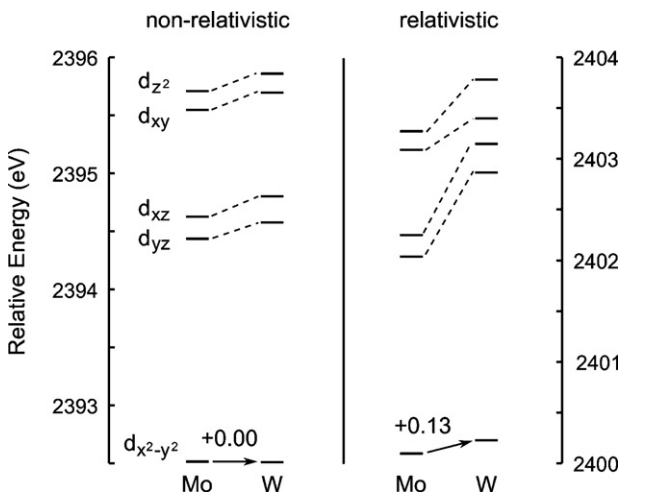

Fig. 11. The five β metal d orbitals of $[MoO(bdt)_2]^{1-}$ and $[WO(bdt)_2]^{1-}$ as determined with non-relativistic (left) and relativistic (right) DFT calculations.

Density functional theory calculations, when validated by comparison with spectroscopic data, can provide additional insight into the origin of fundamental similarities or differences between transition metal complexes. However, any discussion concerning third-row transition metals requires that relativistic effects be considered [5]. As the atomic number increases, the speed of core electrons approaches the relativistic limit. This leads to a mass increase

$$m = \frac{m_0}{\sqrt{1-(v/c)^2}}$$

where m_0 is the rest mass of the electron, v is the speed of the electron, and c is the speed of light, which causes the effective Bohr radius

$$a_0 = \frac{4\pi\varepsilon_0\hbar}{me^2}$$

where ε_0 is the permittivity of free space, $\hbar$ is the reduced Planck constant, and e is the elementary charge, to decrease for core s and p orbitals (*i.e.* a relativistic radial contraction). This has two effects on the electronic structure of a transition metal. First, the valence s and p orbitals also contract to remain orthogonal to the core electrons, and thus, are stabilized in energy. Second, the valence d electrons experience better shielding from the nucleus, resulting in radial expansion and energetic destabilization. Therefore, the Hamiltonian used in DFT calculations of transition metal complexes may need to be modified to include relativistic effects. One simple relativistic perturbation is the inclusion of a scalar mass–velocity term as implemented using the zeroth-order regular approximation (ZORA) [214].

Fig. 11 (left) shows the molecular orbital diagram of the five unoccupied β metal-based orbitals of the $[MO(bdt)_2]^{1-}$ complexes calculated using a non-relativistic Hamiltonian.[2] The orbital splitting pattern is in agreement with the S K-edge data in Fig. 10; *i.e.*, there are three groups of metal-based orbitals: the nonbonding M $d_{x^2-y^2}$, the π anti-bonding d_{xz}/d_{yz}, and the σ anti-bonding d_{xy}/d_{z^2} orbitals. Note, however, that the energy of the W $d_{x^2-y^2}$

[2] Spin-unrestricted DFT calculations allow the α and β wavefunctions to have different spatial distributions, and thus, different energies. The energy splittings for the unoccupied β levels are presented as they are not affected by differences in occupancy.

Table 9
Total compositions of bonding orbitals with O p_z character.

	Non-relativistic		Relativistic	
	$MoOCl_4$	$WOCl_4$	$MoOCl_4$	$WOCl_4$
% M d	40	33	33	36
% M s	8	10	11	17
% M p	2	3	2	3
% O	64	66	69	68
% Cl	87	88	86	82

orbital is equal to that of the Mo $d_{x^2-y^2}$ orbital, and therefore, a non-relativistic Hamiltonian does not reproduce the relative orbital energies observed in the S K-edge data.

Fig. 11 (right) shows the molecular orbital splitting pattern of the five unoccupied β metal d orbitals for $[MO(bdt)_2]^{1-}$ calculated using a Hamiltonian that includes scalar relativistic effects. It also reproduces the orbital splitting pattern observed in the S K-edge data. However, unlike the non-relativistic calculation, the W $d_{x^2-y^2}$ orbital is calculated to be 0.13 eV higher in energy than the Mo $d_{x^2-y^2}$ orbital, in general agreement with the S K-edge data. This demonstrates that inclusion of relativistic effects destabilizes the redox-active orbital in tungsten complexes relative to their molybdenum analogues. Therefore, the experimental trends observed for Mo/W complexes and enzymes, *i.e.,* for redox potentials ($E_W < E_{Mo}$) and rate constants ($k_2^W > k_2^{Mo}$) for oxo transfer to the metal, can be attributed to the greater relativistic effects present in tungsten.

As mentioned in Section 2.4, bond dissociation energies are greater for tungsten complexes compared to their molybdenum analogues (*i.e.* $BDE_W > BDE_{Mo}$) at constant oxidation and ligation. This suggests that, for instance, W=O bonds are stronger than Mo=O bonds. The origin of these differences is considered using the pair $[MOCl_4]$ as an example.

Vibrational frequencies can be used as an indication of the strength of bonds. In the case of $[MOCl_4]$, the experimental frequencies for Mo=O and W=O stretches are 1015 and 1027 cm^{-1} [215], respectively, indicating a stronger W=O bond. Non-relativistic DFT calculations do not reproduce this trend ($\nu_{Mo} = 983\ cm^{-1}$ and $\nu_W = 969\ cm^{-1}$); however, a stronger W=O bond is calculated using relativistic DFT ($\nu_{Mo} = 998$ and $\nu_W = 1011\ cm^{-1}$). Examination of the orbital composition corresponding to the M=O bond provides additional insight into the factors that control the strength of these bonds. There are no significant differences for metal contribution to the bonding π orbitals with predominately O p_x/p_y character, however, there is for the σ bond. The composition of the filled valence molecular orbital formed from interactions with the O p_z orbital is given in Table 9. The non-relativistic calculations show a decrease (4%) in total metal character in going from Mo to W, which is consistent with the lower W=O stretching frequency calculated with a non-relativistic Hamiltonian. In contrast, the relativistic calculations show an increase (4%) in M character in going from Mo to W (consistent with the larger W=O stretching frequency), with the M s orbital contributing the largest change (increase of 6%). Note that inclusion of relativistic effects increases the amount of W s character by 7%, which is the result of the energetic stabilization of the W 6s orbital due to radial contraction.

- *The fundamental differences between molybdenum and tungsten can, at least in part, be attributed to larger relativistic effects in the later. Specifically, the relativistic destabilization of the metal d orbitals influences reduction potentials ($E_W < E_{Mo}$) and reaction rates for oxo transfer to the metal ($k_2^W > k_2^{Mo}$), while the relativistic contraction of metal s orbitals influences the bond strengths ($BDE_W > BDE_{Mo}$) and vibrational frequencies ($\nu_W > \nu_{Mo}$).*

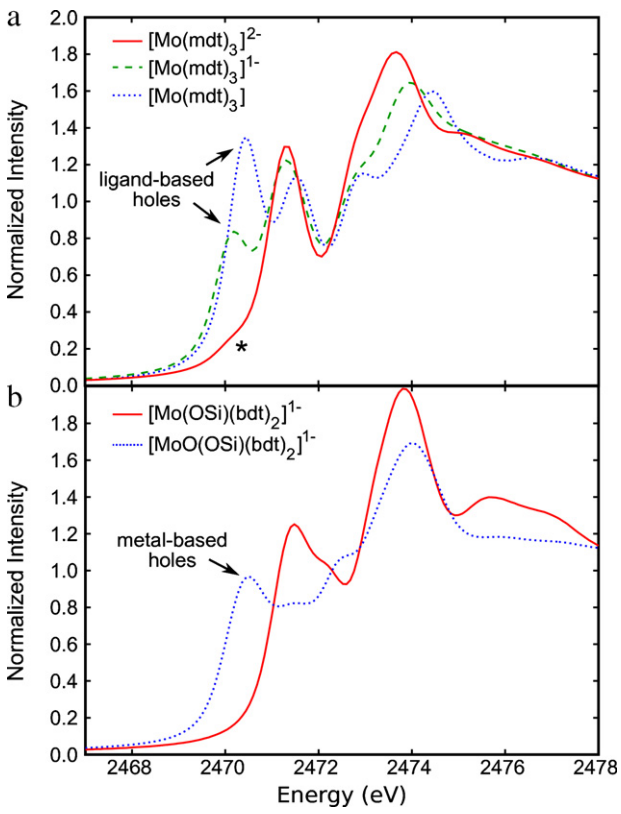

Fig. 12. The sulfur K-edge XAS data for (a) the dianionic, monoanionic, and neutral Mo tris-dithiolene complexes (solid red, dashed green, and dotted blue, respectively), and (b) the Mo(IV) and Mo(VI) = O bis-dithiolene complexes (solid red and dotted blue, respectively). The asterisk in (a) indicates an oxidized impurity. Note that the data are normalized such that the intensity of the post-edge region is 1.0, and thus, the tris-dithiolene data (6 sulfur atoms) need to be scaled by 1.5 for direct comparison to the bis-dithiolene data (4 sulfur atoms).

5.3. *Mechanism of a functional analogue of DMSO and TMNO reductases*

Functional analogues of DMSOR and TMNOR have been prepared in the Harvard laboratories (Section 4). The electronic structures of these complexes were determined using sulfur K-edge XAS which provides a direct probe of metal–ligand bonding [216,217]. Specifically, the intensity (D_0) of pre-edge features can be used to determine the amount of sulfur character (*i.e.*, covalency) in unfilled molecular orbitals with metal d character

$$D_0(\mathrm{S\ 1s} \rightarrow \psi*) = \mathrm{const}|\langle \mathrm{S\ 1s}|\mathbf{r}|\psi*\rangle|^2 = (\alpha^2 h/3n)I_s$$

where **r** is the electric dipole operator, $\psi^* = (1-\alpha^2)^{1/2}|M_d\rangle - \alpha|S_{3p}\rangle$ (*i.e.,* the antibonding orbital reflecting the metal–ligand bonding), α^2 is the covalency, h is the number of holes in the acceptor orbital to account for spin/orbital degeneracy, n is the number of sulfur atoms which accounts for the normalization procedure, and I_s is the intensity of the electric-dipole allowed S 1s → S 3p transition which is estimated from experimental S K-edge data. Therefore, the sulfur character in a molecular orbital is directly proportional to the intensity of its corresponding pre-edge feature.

Before discussing the electronic structures of functional models of DMSOR and TMNOR, it is important to understand Mo–S bonding without the complication of an oxo ligand. Therefore, the tris(dithiolene) complexes $[Mo(mdt)_3]^z$ (z = 2-, 1-, 0) are considered briefly [216]. The sulfur K-edge data are presented in Fig. 12a. In going from the dianion (red) to the monoanion (dashed green) and the neutral (dotted blue) complex, a new pre-edge feature appears at ~2470 eV corresponding to the holes created due to one-

and two-electron oxidation, respectively. The intensities of these new pre-edge features indicate that the corresponding orbitals have 75% and 69% S 3p character, respectively. Therefore, the Mo tris(dithiolene) complexes undergo ligand-based oxidation, and thus, the dithiolene ligands have non-innocent interactions with the molybdenum atom.

The complexes $[Mo^{IV}(OSiPh_2Bu^t)(bdt)_2]^{1-}$ and $[Mo^{VI}O(OSiPh_2Bu^t)(bdt)_2]^{1-}$ [43], designated as $[Mo(OSi)(bdt)_2]^{1-}$ and $[MoO(OSi)(bdt)_2]^{1-}$, respectively, serve as analogues of the catalytic site in DMSORs in a detailed spectroscopic and calculational examination of the oxo atom transfer process [217]. The sulfur K-edge data for $[Mo(OSi)(bdt)_2]^{1-}$ (solid red) and $[MoO(OSi)(bdt)_2]^{1-}$ (dotted blue) are shown in Fig. 12b. Note that in comparing these data to those of the tris(dithiolenes), the intensities in Fig. 12a should be scaled by 1.5 to account for the different number of sulfur atoms, *i.e.,* six in the tris(dithiolene) versus four in the bis(dithiolene) complexes. There are two key observations. First, oxidation of the Mo^{IV} des-oxo complex results in a new pre-edge feature at ~2470 eV in the data of the $Mo^{VI}O$ bis(dithiolene) complex due to the two holes created upon oxidation. Second, the intensity of this pre-edge feature corresponds to an unfilled orbital with 32% S 3p character (*i.e.,* metal-based orbital). This is significantly less than 69% S 3p observed for the ligand-based orbital of $[Mo(mdt)_3]$ (dotted blue line in Fig. 12a). Note that there is also a decrease in intensity (*i.e.* covalency) of the metal-based peaks at higher energy for the $Mo^{VI}O$ complex. Therefore, the dithiolene ligands are behaving innocently in this complex in contrast to the non-innocent interactions seen in the tris(dithiolenes).

The molecular orbital diagrams for $[Mo(OSi)(bdt)_2]^{1-}$ (left) and $[MoO(OSi)(bdt)_2]^{1-}$ (right) as determined by DFT calculations are shown in Fig. 13. The coordinate system is chosen such that the *x* and *y* axes bisect the S–Mo–S angles and the *z* axis is along the Mo–O or Mo=O bond (des-oxo or monooxo, respectively). The lowest energy orbital in both complexes is the Mo $d_{x^2-y^2}$ orbital, which becomes unoccupied in going to the $Mo^{VI}O$ complex in agreement with the sulfur K-edge XAS data. Next are the d_{yz}/d_{xz} orbitals that have anti-bonding interactions with the dithiolene out-of-plane S p orbitals and the O p_x and p_y orbitals. The Mo d_{xy} and d_{z^2} orbitals are at higher energies and have σ anti-bonding interactions with the

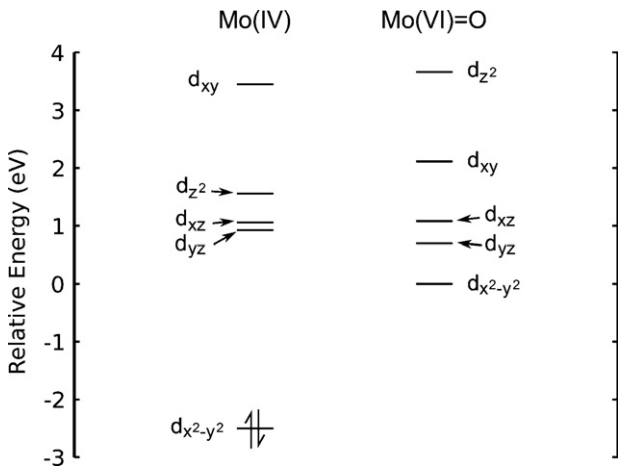

Fig. 13. The molecular orbital diagram of the Mo(IV) and Mo(VI)=O bis-dithiolene complexes (left and right, respectively). The energy levels are shifted such that the relative LUMO energies reflect the differences seen in the sulfur K-edge data.

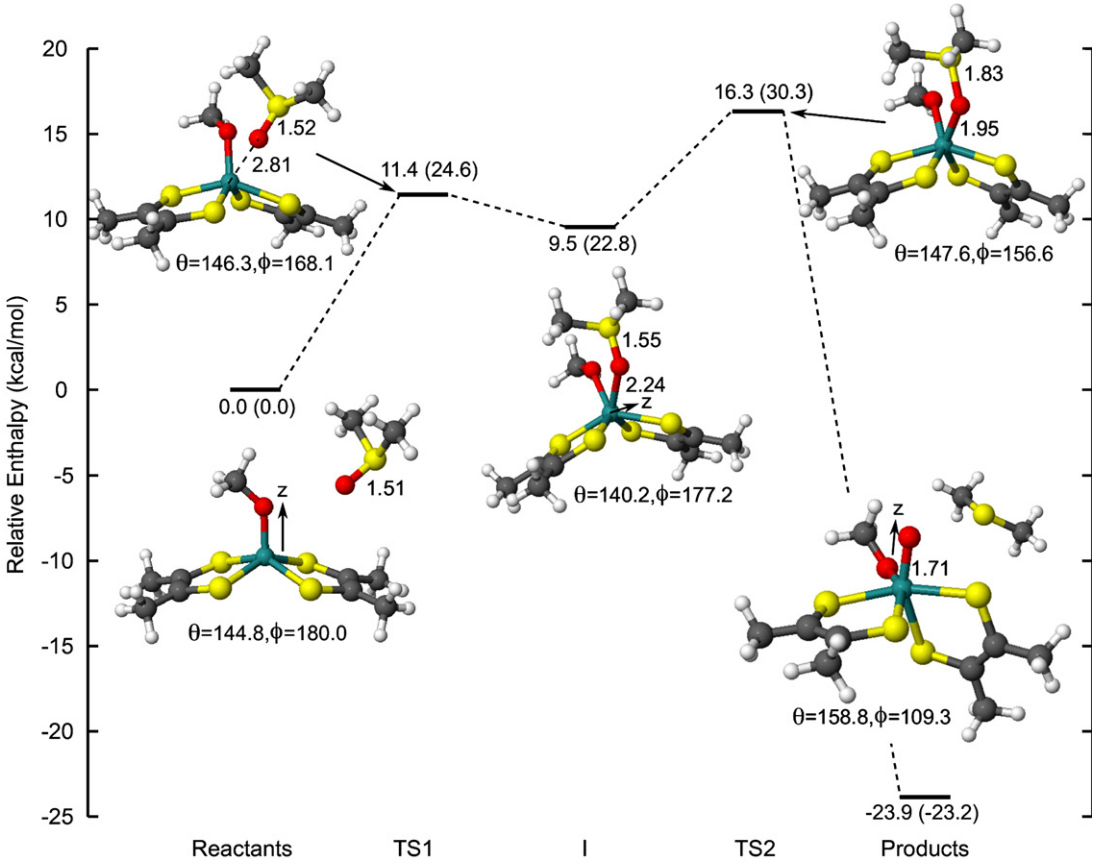

Fig. 14. The reaction coordinate for oxo transfer from DMSO to a Mo(IV) bis-dithiolene complex $[Mo(OMe)(mdt)_2]^{1-}$. Values in parentheses are Gibbs free energies. The structural parameters θ and φ are defined as the largest S_2–Mo–S_3 angle (S_2 and S_3 are on different dithiolenes) and S_1–S_2–S_3–S_4 dihedral angle, respectively. Square pyramidal and trigonal prismatic geometries are given by $\theta < 180^\circ$ and $\phi = 180^\circ$ while an octahedral geometry has $\theta = 180^\circ$ and $\varphi = 90^\circ$. Bond distances are in Å. Adapted from ref. [217].

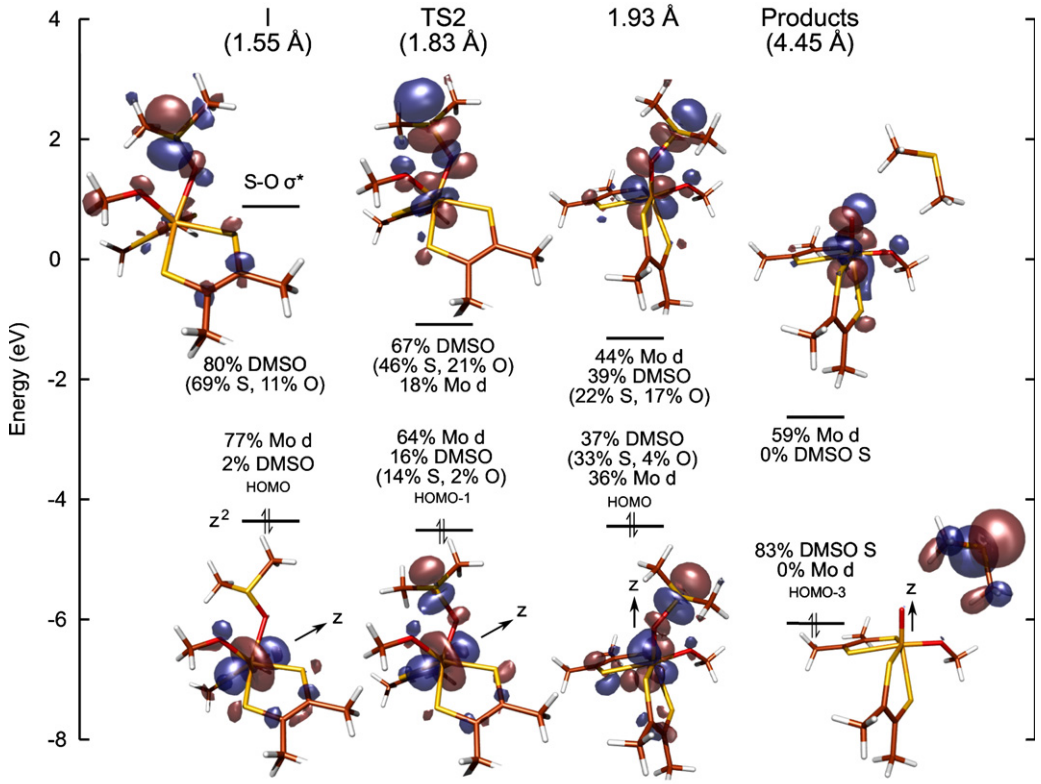

Fig. 15. The frontier molecular orbitals (FMOs) involved in oxo transfer at certain points along the reaction coordinate (distances refer to S–O bond length (Å)). The occupied FMO is a non-bonding Mo orbital and the unoccupied FMO is the DMSO S–O σ* orbital. Note that little electron density has been transferred at the second transition state (TS2). Adapted from ref. [217].

dithiolene in-plane S p and O p_z orbitals, respectively. Note that the energetic ordering of these orbitals is switched between the two complexes due to the strong oxo ligand in the $Mo^{VI}O$ complex which destabilizes the d_{z^2} orbital relative to the d_{xy} orbital.

These experimentally calibrated DFT calculations have been extended to determine the oxo transfer reaction coordinate from DMSO to a similar but calculationally simpler Mo^{IV} bis(dithiolene) complex (Fig. 14). The first transition state (TS1) is due to the distortion of the alkoxyl ligand away from the axial position to accommodate the incoming DMSO substrate, resulting in an intermediate (*I*) with DMSO weakly bound (Mo–S distance of 2.24 Å). Note that the DMSO S–O bond length at I (1.55 Å) is similar to that of free DMSO (1.51 Å), indicating that essentially no oxo transfer has occurred at this state. The second transition state (TS2), which is also the largest barrier ($\Delta H^{\ddagger}$ = 16.3 kcal/mol), results from the lengthening of the DMSO S–O bond (1.83 Å) necessary for oxo transfer.

Examination of the frontier molecular orbitals (FMOs) involved in oxo transfer around TS2 (Fig. 15) provides valuable insight into the mechanism of oxo transfer. Starting at the DMSO-bound intermediate (*I*), two electrons are present in a non-bonding Mo d_{z^2} orbital, and the S–O σ* orbital is unoccupied. Note that *I* is a six-coordinate trigonal prism and the Mo d_{z^2} orbital is now oriented along the approximate C_3 rotation axis and is non-bonding in this geometry. As the S–O distance is increased upon going to TS2, these orbitals begin to undergo configuration interaction (*i.e.* orbital mixing) with some electron density transferred to the S–O σ* as seen by its additional character (16%) in the occupied FMO. A corresponding increase in Mo d character is present in the unoccupied FMO. However, it is not until the S–O distance has been increased past TS2 to 1.93 Å that the majority of the occupied FMO has S–O σ* character. This orbital mixing continues until the electron pair has been transferred into a S 3p orbital and the oxo has been transferred to the Mo complex. These results show that *electron transfer does not occur until after TS2* (*i.e.* the rate-limiting step) indicating that there should be little, if any, correlation between the redox potential of the M^{IV} complex and the rate of oxo transfer in agreement with experimental results [192].

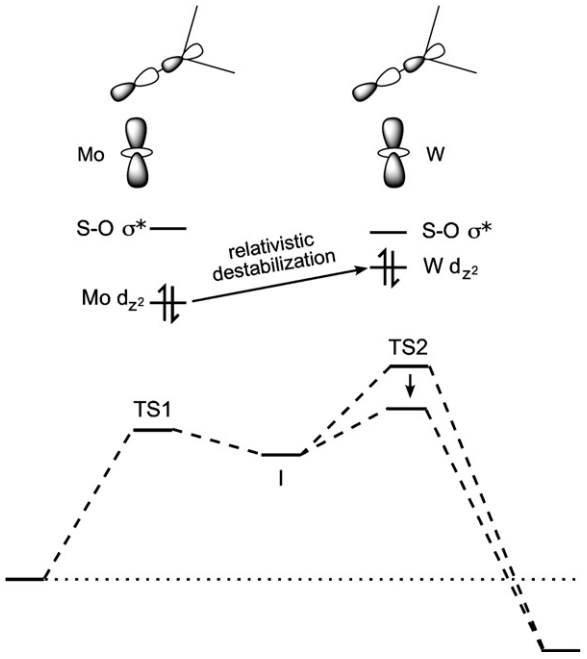

Fig. 16. In going from Mo to W, the non-bonding metal d_{z^2} orbital will become destabilized due to relativistic effects. This decreases the energetic separation between the FMOs, which stabilizes TS2 and accelerates oxo transfer. Adapted from ref. [217].

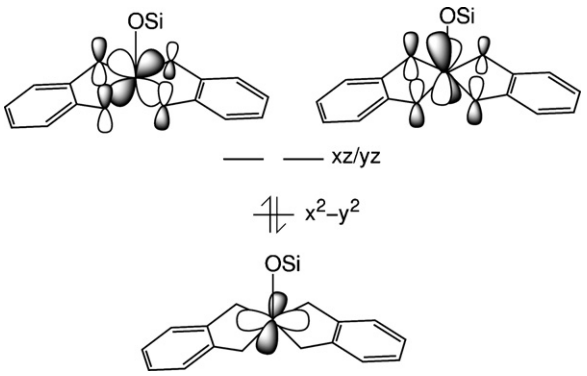

Fig. 17. The dithiolene C=C bond orients the out-of-plane S p orbitals such that they can only interact with Mo d_{xz}/d_{yz} orbitals. This π anisotropy destabilizes these orbitals relative to the Mo $d_{x^2-y^2}$ orbital, which stabilizes a singlet ground state. Adapted from ref. [217].

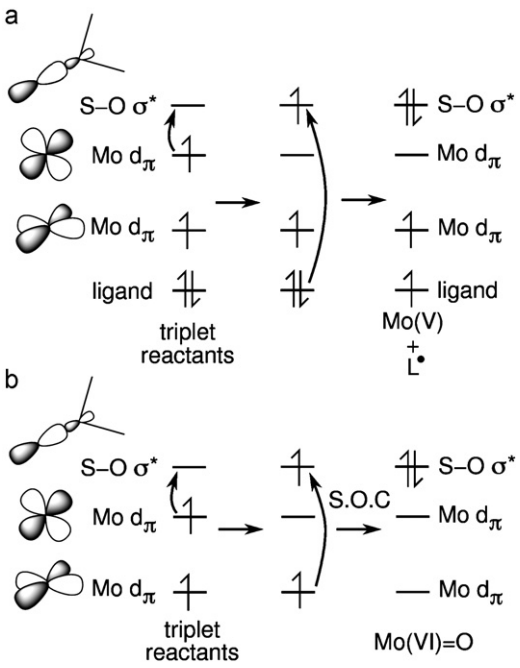

Fig. 18. (a) A triplet Mo(IV) reactant would result in an unfavorable Mo(V) site with a ligand radical, and (b) intersystem crossing between the singlet and triplet surfaces would be inefficient due to poor spin–orbit coupling as the orbitals involved are dominantly centered on different atoms.

This oxo transfer reaction coordinate also provides insight into the observation that oxo transfer to tungsten sites is faster than to analogous molybdenum sites (Section 4.2). Since the mechanism of oxo transfer from DMSO to the Mo^{IV} bis(dithiolene) involves the configuration interaction of a non-bonding Mo d orbital and the S–O σ* at the rate-limiting TS2, decreasing the energetic separation of these orbitals would facilitate this orbital mixing, and thus, lower the energy of this barrier. As was shown in Section 5.2, W d orbitals are destabilized relative to Mo d orbitals due to relativistic effects. Therefore, the energy of TS2 will be lower for oxo transfer to W^{IV} sites than to Mo^{IV} sites (Fig. 16), and indeed, this was demonstrated in a separate computational study [218].

Finally, any examination of dithiolene complexes that are functional analogues of molybdenum and tungsten enzymes would be incomplete without discussion of the role of the pterin-dithiolene cofactor (**1** in Fig. 2). It appears that one important role of the dithiolene chelate is to stabilize a singlet ground state in the des-oxo Mo^{IV} site. Mo^{IV} complexes without oxo ligands sometimes have triplet ground states due to the limiting splitting of the Mo dπ orbitals. However, the C=C bond in dithiolene ligands orients the S out-of-plane orbitals such that they can only interact with the Mo d_{xz}/d_{yz} orbitals. This π anisotropy destabilizes these orbitals relative to the Mo $d_{x^2-y^2}$ orbital, which stabilizes a singlet ground state for the Mo^{IV} des-oxo site (Fig. 17). This singlet ground state persists along the oxo transfer reaction coordinate.

The singlet ground state for the Mo^{IV} des-oxo site is important for two reasons. First, the mechanism of oxo transfer described above and elsewhere [217], requires the transfer of two electrons from a non-bonding Mo d orbital to the S–O σ* orbital. If the Mo^{IV}

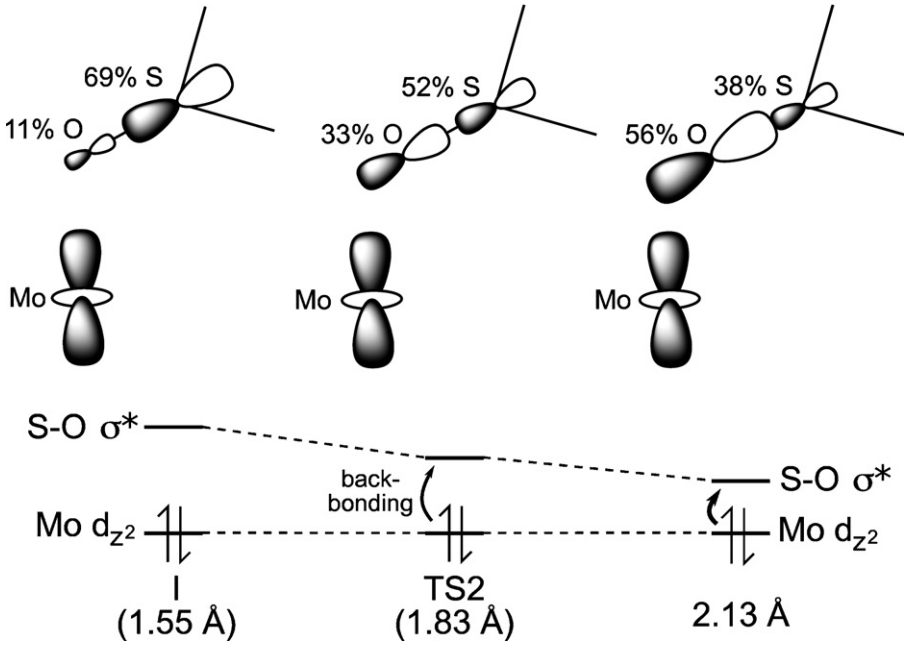

Fig. 19. Oxo transfer occurs by the configurational interaction between the filled, non-bonding Mo d_{z^2} orbital and the unoccupied DMSO S–O σ* orbital. As the S–O bond is lengthened, the S–O σ* orbital is stabilized and its oxygen character increases. This leads to better overlap between the two FMOs further facilitating electron transfer and S–O bond cleavage. Adapted from ref. [217].

des-oxo site had a triplet ground state that persisted along the reaction coordinate, then only one α dπ electron could be transferred from the Mo center to the S–O σ* orbital. The β electron would then have to be from the dithiolene ligands which would result in an energetically unfavorable Mo^{V} site with a ligand radical (Fig. 18a). Second, oxo transfer to a triplet Mo^{IV} des-oxo site resulting in a singlet $Mo^{VI}O$ site would require intersystem crossing between singlet and triplet surfaces. Such intersystem crossing depends upon efficient spin–orbit coupling from an occupied α orbital to an unoccupied β orbital (Fig. 18b). However, since spin–orbit coupling is dominantly a single-center operator, efficient spin–orbit coupling requires that these orbitals be on the same atom. Calculations indicate that the singlet and triplet surfaces cross late along the reaction coordinate for triplet Mo^{IV} complexes such as $[Mo(OMe)Cl_4]^{1-}$. At this crossing point, the occupied α orbital is metal-based while the unoccupied β orbital has mostly S–O σ* character, and thus, intersystem crossing between the singlet and triplet surfaces would be inefficient. Therefore, one important role of the dithiolene ligand in these enzymes and models appears to be the stabilization of a singlet ground state in Mo^{IV} des-oxo sites for efficient oxo transfer.

- *Oxo transfer involves the configuration interaction between a filled Mo d_{z^2} orbital (non-bonding in the trigonal prismatic geometry of the substrate-bound intermediate) and the unoccupied DMSO S–O σ* orbital (Fig. 19). As the S–O bond is lengthened, the S–O σ* FMO is stabilized and the oxygen character increases (reflecting some electron transfer from oxygen to sulfur). These orbital changes lead to better overlap between the occupied Mo d_{z^2} and unoccupied S–O σ* orbitals, which further facilitates electron transfer from the metal into this oxygen-polarized σ* orbital and S–O bond cleavage.*

Acknowledgments

Research at Harvard University on the biomimetic chemistry of molybdenum and tungsten has been supported by the National Science Foundation (currently grant CHE 0846397), and investigations at Stanford University of spectroscopy and electronic structural correlations with reactivity by the National Science Foundation under grant CHE 0948211.

References

[1] C.F. Baes Jr., R.E. Mesmer, The Hydrolysis of Cations, Wiley Interscience, New York, 1974, p. 253.
[2] O.F. Oyerinde, C.L. Weeks, A.D. Anbar, T.G. Spiro, Inorg. Chim. Acta 361 (2008) 1000.
[3] J. Emsley, The Elements, Oxford University Press, Oxford, 1998.
[4] G.C. Tucci, J.P. Donahue, R.H. Holm, Inorg. Chem. 37 (1998) 1602.
[5] P. Pyykkö, Chem. Rev. 88 (1988) 563.
[6] R. Hille, Chem. Rev. 96 (1996) 2757.
[7] H. Schindelin, C. Kisker, K.V. Rajagopalan, Adv. Protein Chem. 58 (2001) 47.
[8] R. Hille, Eur. J. Inorg. Chem. (2006) 1913.
[9] M.J. Romão, Dalton Trans. (2009) 4053.
[10] M.K. Johnson, D.C. Rees, M.W.W. Adams, Chem. Rev. 96 (1996) 2817.
[11] A. Kletzin, M.W.W. Adams, FEMS Microbiol. Rev. 18 (1996) 5.
[12] W.R. Hagen, A.F. Arendsen, Struct. Bond. 90 (1998) 161.
[13] L.E. Bevers, P.-L. Hagedoorn, W.R. Hagen, Coord. Chem. Rev. 253 (2008) 269.
[14] J.H. Enemark, J.J.A. Cooney, J.-J. Wang, R.H. Holm, Chem. Rev. 104 (2004) 1175.
[15] J. McMaster, J.T. Tunney, C.D. Garner, Prog. Inorg. Chem. 52 (2004) 539.
[16] H. Sugimoto, H. Tsukube, Chem. Soc. Rev. 37 (2008) 2609.
[17] S. Groysman, R.H. Holm, Biochemistry 48 (2009) 2310.
[18] M. Minelli, J.H. Enemark, R.T.C. Brownlee, M.J. O'Connor, A.G. Wedd, Coord. Chem. Rev. 68 (1985) 169.
[19] J. Malito, Annu. Rep. NMR Spectrosc. 33 (1997) 2310.
[20] K. Niki, in: A.J. Bard, R. Parsons, J. Jordan (Eds.), Standard Potentials in Aqueous Solution, Marcel Dekker, Inc., New York, 1985 (Chap. 16).
[21] K.S. Pitzer, Acc. Chem. Res. 12 (1979) 271.
[22] C.L. Beswick, J.M. Schulman, E.I. Stiefel, Prog. Inorg. Chem. 52 (2004) 55.
[23] D.V. Partyka, R.H. Holm, Inorg. Chem. 43 (2004) 8609.
[24] S. Groysman, J.-J. Wang, R. Tagore, S.C. Lee, R.H. Holm, J. Am. Chem. Soc. 130 (2008) 12794.
[25] B.S. Lim, M.W. Willer, M. Miao, R.H. Holm, J. Am. Chem. Soc. 123 (2001) 8343.
[26] J.-J. Wang, R.H. Holm, Inorg. Chem. 46 (2007) 11156.
[27] H. Oku, N. Ueyama, A. Nakamura, Y. Kai, N. Kanehisa, Chem. Lett. (1994) 607.
[28] S.K. Das, P.K. Chaudhury, D. Biswas, S. Sarkar, J. Am. Chem. Soc. 116 (1994) 9061.
[29] H. Oku, N. Ueyama, A. Nakamura, Inorg. Chem. 34 (1995) 3667.
[30] S.K. Das, D. Biswas, R. Maiti, S. Sarkar, J. Am. Chem. Soc. 118 (1996) 1387.
[31] B. Götz, F. Knoch, H. Kisch, Chem. Ber. 129 (1996) 33.
[32] H. Oku, N. Ueyama, A. Nakamura, Inorg. Chem. 36 (1997) 1504.
[33] H. Sugimoto, M. Tarumizu, K. Tanaka, H. Miyake, H. Tsukube, J. Chem. Soc., Dalton Trans. (2005) 3558.
[34] C. Schulzke, J. Chem. Soc., Dalton Trans. (2005) 713.
[35] S. Sarkar, S.K. Das, Proc. Indian Acad. Sci. (Chem. Sci.) 104 (1992) 533.
[36] K. Wang, J.M. McConnachie, E.I. Stiefel, Inorg. Chem. 38 (1999) 4334.
[37] B.S. Lim, J.P. Donahue, R.H. Holm, Inorg. Chem. 39 (2000) 263.
[38] K.-M. Sung, R.H. Holm, Inorg. Chem. 40 (2001) 4518.
[39] N. Ueyama, T. Okamura, A. Nakamura, J. Am. Chem. Soc. 114 (1992) 8129.
[40] H. Oku, N. Ueyama, M. Kondo, A. Nakamura, Inorg. Chem. 33 (1994) 209.
[41] S. Boyde, S.R. Ellis, C.D. Garner, W. Clegg, J. Chem. Soc., Chem. Commun. (1986) 1541.
[42] J.P. Donahue, C. Lorber, E. Nordlander, R.H. Holm, J. Am. Chem. Soc. 120 (1998) 3259.
[43] J.P. Donahue, C.R. Goldsmith, U. Nadiminti, R.H. Holm, J. Am. Chem. Soc. 120 (1998) 12869.
[44] H. Sugimoto, K. Suyama, K. Sugimoto, H. Miyake, I. Takahashi, S. Hirota, S. Itoh, Inorg. Chem. 47 (2008) 10150.
[45] A.L. Tenderholt, R.K. Szilagyi, R.H. Holm, K.O. Hodgson, B. Hedman, E.I. Solomon, J. Inorg. Biochem. 101 (2007) 1594.
[46] R.L. McNaughton, M.E. Helton, N.D. Rubie, M.L. Kirk, Inorg. Chem. 39 (2000) 4386.
[47] D. Coucouvanis, A. Hadjikyriacou, A. Toupadakis, S.-M. Koo, O. Ileperuma, M. Draganjac, A. Salifoglou, Inorg. Chem. 30 (1991) 754.
[48] R.S. Pilato, E.I. Stiefel, in: J. Reedjik, E. Bouwman (Eds.), Bioinorganic Catalysis, Marcel Dekker, Inc., New York, 1999, p. 81.
[49] S. Groysman, R.H. Holm, Inorg. Chem. 46 (2007) 4090.
[50] H. Tano, R. Tajima, H. Miyake, S. Itoh, H. Sugimoto, Inorg. Chem. 47 (2008) 7465.
[51] J.-J. Wang, C. Tessier, R.H. Holm, Inorg. Chem. 45 (2006) 2979.
[52] B.S. Lim, R.H. Holm, J. Am. Chem. Soc. 123 (2001) 1920.
[53] K.-M. Sung, R.H. Holm, J. Am. Chem. Soc. 123 (2001) 1931.
[54] R.L. McNaughton, B.S. Lim, S.Z. Knottenbelt, R.H. Holm, M.L. Kirk, J. Am. Chem. Soc. 130 (2008) 4628.
[55] B.S. Lim, K.-M. Sung, R.H. Holm, J. Am. Chem. Soc. 122 (2000) 7410.
[56] K.-M. Sung, R.H. Holm, Inorg. Chem. 39 (2000) 1275.
[57] J.-J. Wang, O. Kryatova, E.V. Rybak-Akimova, R.H. Holm, Inorg. Chem. 43 (2004) 8092.
[58] J. Jiang, R.H. Holm, Inorg. Chem. 44 (2005) 1068.
[59] C. Lorber, J.P. Donahue, C.A. Goddard, E. Nordlander, R.H. Holm, J. Am. Chem. Soc. 120 (1998) 8102.
[60] J. Jiang, R.H. Holm, Inorg. Chem. 43 (2004) 1302.
[61] G.N. Schrauzer, V.P. Mayweg, W. Heinrich, J. Am. Chem. Soc. 88 (1966) 5174.
[62] C.A. Goddard, R.H. Holm, Inorg. Chem. 38 (1999) 5389.
[63] D.V. Fomitchev, B.S. Lim, R.H. Holm, Inorg. Chem. 40 (2001) 645.
[64] P. Chandrasekaran, K. Arumugam, U. Jayarathne, L.M. Pérez, J.T. Mague, J.P. Donahue, Inorg. Chem. 48 (2009) 2103.
[65] N.G. Connelly, J. Locke, J.A. McCleverty, D.A. Phipps, B. Ratcliff, Inorg. Chem. 9 (1970) 278.
[66] N.J. Lazarowych, R.H. Morris, Can. J. Chem. 68 (1990) 558.
[67] T.E. Burrow, R.H. Morris, A. Hills, D.L. Hughes, R.L. Richards, Acta Crystallogr. C49 (2009) 1591.
[68] N. Ueyama, H. Oku, M. Kondo, T. Okamura, N. Yoshinaga, A. Nakamura, Inorg. Chem. 35 (1996) 643.
[69] C. Lorber, M.R. Plutino, L.I. Elding, E. Nordlander, J. Chem. Soc., Dalton Trans. (1997) 3997.
[70] N. Yoshinaga, N. Ueyama, T. Okamura, A. Nakamura, Chem. Lett. (1990) 1655.
[71] N. Ueyama, H. Oku, A. Nakamura, J. Am. Chem. Soc. 114 (1992) 7310.
[72] A.E. Smith, G.N. Schrauzer, V.P. Mayweg, W. Heinrich, J. Am. Chem. Soc. 87 (1965) 5798.
[73] G.N. Schrauzer, V.P. Mayweg, J. Am. Chem. Soc. 88 (1966) 3235.
[74] D.C. Olson, V.P. Mayweg, G.N. Schrauzer, J. Am. Chem. Soc. 88 (1966) 4876.
[75] J.A. McCleverty, J. Locke, E.J. Wharton, M. Gerloch, J. Chem. Soc. (A) (1968) 816.
[76] E.I. Stiefel, L.E. Bennett, Z. Dori, T.H. Crawford, C. Simo, H.B. Gray, Inorg. Chem. 9 (1970) 281.
[77] E.I. Stiefel, R. Eisenberg, R.C. Rosenberg, H.B. Gray, J. Am. Chem. Soc. 88 (1966) 2956.
[78] A. Davison, N. Edelstein, R.H. Holm, A.H. Maki, J. Am. Chem. Soc. 86 (1964) 2799.
[79] R.B. King, Inorg. Chem. 2 (1963) 641.
[80] G. Matsubayashi, K. Douki, H. Tamura, Chem. Lett. (1992) 1251.
[81] G. Matsubayashi, K. Douki, H. Tamura, M. Nakano, W. Mori, Inorg. Chem. 32 (1993) 5990.
[82] P. Falaras, C.-A. Mitsopoulou, D. Argyropoulos, E. Lyria, N. Psaroudakis, E. Vrachnou, D. Katakis, Inorg. Chem. 34 (1995) 4536.
[83] S. Boyde, C.D. Garner, J.A. Joule, D.J. Rowe, J. Chem. Soc., Chem. Commun. (1987) 800.
[84] D. Argyropoulos, E. Lyris, C. Mitsopoulou, D. Katakis, J. Chem. Soc., Dalton Trans. (1997) 615.

[85] M. Cowie, M.J. Bennett, Inorg. Chem. 15 (1976) 1584.
[86] D. Sellman, L. Zapf, Z. Naturforsch. 40b (1985) 380.
[87] D. Sellmann, W. Kern, M. Moll, J. Chem. Soc., Dalton Trans. (1991) 1733.
[88] A. Cervilla, E. Llopis, D. Marco, F. Pérez, Inorg. Chem. 40 (2001) 6525.
[89] C.S. Isfort, T. Pape, F.E. Hahn, Eur. J. Inorg. Chem. (2005) 2607.
[90] R.R. Kapre, E. Bothe, T. Weyhermüller, S.D. George, K. Wieghardt, Inorg. Chem. 46 (2007) 5642.
[91] H. Sugimoto, Y. Furukawa, M. Tarumizu, H. Miyake, K. Tanaka, H. Tsukube, Eur. J. Inorg. Chem. (2005) 3088.
[92] T.A. James, J.A. McCleverty, J. Chem. Soc. (A) (1970) 3308.
[93] E.J. Wharton, J.A. McCleverty, J. Chem. Soc. (A) 2258 (1969) 2266.
[94] C.J. Doonan, A. Stockert, R. Hille, G.N. George, J. Am. Chem. Soc. 127 (2005) 4518.
[95] G.N. George, C.J. Doonan, R.A. Rothery, N. Boroumand, J.H. Weiner, Inorg. Chem. 46 (2007) 2.
[96] K.B. Musgrave, J.P. Donahue, C. Lorber, R.H. Holm, B. Hedman, K.O. Hodgson, J. Am. Chem. Soc. 121 (1999) 10297.
[97] K.B. Musgrave, B.S. Lim, K.-M. Sung, R.H. Holm, B. Hedman, K.O. Hodgson, Inorg. Chem. 39 (2000) 5238.
[98] F. Jalilehvand, B.S. Lim, R.H. Holm, B. Hedman, K.O. Hodgson, Inorg. Chem. 42 (2003) 5531.
[99] M.H. Chisholm, D.M. Hoffman, J.C. Huffman, Inorg. Chem. 22 (1983) 2903.
[100] D.M.T. Chan, M.H. Chisholm, K. Folting, J.C. Huffman, N.S. Marchant, Inorg. Chem. 25 (1986) 4170.
[101] D.S. Kuiper, R.E. Douthwaite, A.-R. Mayol, P.T. Wolczanski, E.B. Lobkovsky, T.R. Cundari, O.P. Lam, K. Meyer, Inorg. Chem. 47 (2008) 7139.
[102] N.L. Kruhlak, M. Wang, P.M. Boorman, M. Parvez, R. McDonald, Inorg. Chem. 40 (2001) 3141.
[103] K.E. Lewis, D.M. Golden, G.P. Smith, J. Am. Chem. Soc. 106 (1984) 3905.
[104] J. Li, G. Schreckenbach, T. Ziegler, J. Phys. Chem. 98 (1994) 4838.
[105] Y.-J. Chen, C.-L. Liao, C.Y. Ng, J. Chem. Phys. 107 (1997) 4527.
[106] G. Frenking, K. Wichman, N. Froehlich, J. Grobe, W. Golla, D.L. Van, B. Krebs, M. Laege, Organometallics 21 (2002) 2921.
[107] D.J. Darensbourg, A.H. Graves, Inorg. Chem. 18 (1979) 1257.
[108] I. Cacelli, R. Poli, E.A. Quadrelli, A. Rizzo, K.M. Smith, Inorg. Chem. 39 (2000) 517.
[109] J.E. McDonough, J.J. Weir, K. Sukcharoenphon, C.D. Hoff, O.P. Kryatova, E.V. Rybak-Akimova, B.L. Scott, G.J. Kubas, A. Mendiratta, C.C. Cummins, J. Am. Chem. Soc. 128 (2006) 10295.
[110] J.C. Bryan, J.M. Mayer, J. Am. Chem. Soc. 112 (1990) 2298.
[111] L. Luo, G. Lanza, I.L. Fragalà, C.L. Stern, T.J. Marks, J. Am. Chem. Soc. 120 (1998) 3111.
[112] V.N. Nemykin, J. Laskin, P. Basu, J. Am. Chem. Soc. 126 (2004) 8604.
[113] J.-P.F. Cherry, A.R. Johnson, L.M. Baraldo, Y.-C. Tsai, C.C. Cummins, S.V. Kryatov, E.V. Rybak-Akimova, K.B. Capps, C.D. Hoff, C.M. Haar, S.P. Nolan, J. Am. Chem. Soc. 123 (2001) 7271.
[114] F.H. Stephens, M.J.A. Johnson, C.C. Cummins, O.P. Kryatova, S.V. Kryatov, E.V. Rybak-Akimova, J.E. McDonough, C.D. Hoff, J. Am. Chem. Soc. 127 (2005) 15191.
[115] H.S. Soo, J.S. Figueroa, C.C. Cummins, J. Am. Chem. Soc. 126 (2004) 11370.
[116] K.G. Dyall, J. Phys. Chem. A 104 (2000) 4077.
[117] A.R. Johnson, W.M. Davis, C.C. Cummins, S. Serron, S.P. Nolan, D.G. Musaev, K. Morokuma, J. Am. Chem. Soc. 120 (1998) 2071.
[118] J.E. McDonough, A. Mendiratta, J.J. Curley, G.C. Fortman, S. Fantasia, C.C. Cummins, E.V. Rybak-Akimova, S.P. Nolan, C.D. Hoff, Inorg. Chem. 47 (2008) 2133.
[119] G.D. Watt, J.W. McDonald, W.E. Newton, J. Less-Common Met. 54 (1977) 415.
[120] R.H. Holm, J.P. Donahue, Polyhedron 12 (1993) 571.
[121] O. Gonsález-Blanco, V. Branchadell, K. Monteyne, T. Ziegler, Inorg. Chem. 37 (1998) 1744.
[122] K.H. Moock, M.H. Rock, J. Chem. Soc., Dalton Trans. (1993) 2459.
[123] K.H. Moock, S.A. Macgregor, G.A. Heath, S. Derrick, R.T. Boeré, J. Chem. Soc., Dalton Trans. (1996) 2067.
[124] A. Dõring, C. Schultzke, Dalton Trans. 39 (2010) 5623.
[125] G.A. Heath, K.A. Moock, D.W.A. Sharp, L.J. Yellowlees, J. Chem. Soc., Chem. Commun. (1985) 1503.
[126] S.-L. Soong, V. Chebolu, S.A. Koch, T.O. O'Sullivan, M. Millar, Inorg. Chem. 25 (1986) 4067.
[127] G. Backes-Dahmann, W. Herrmann, K. Wieghardt, J. Weiss, Inorg. Chem. 24 (1985) 485.
[128] G. Backes-Dahmann, K. Wieghardt, Inorg. Chem. 24 (1985) 4049.
[129] M. Millar, S.H.C.J. Lincoln, S.A. Koch, J. Am. Chem. Soc. 104 (1982) 288.
[130] D. Hong, Y. Zhang, R.H. Holm, Inorg. Chim. Acta 358 (2005) 2303.
[131] H.-C. Zhou, W. Su, C. Achim, P.V. Rao, R.H. Holm, Inorg. Chem. 41 (2002) 3191.
[132] D.A. Smith, B. Zhuang, W.E. Newton, J.W. McDonald, F.A. Shultz, Inorg. Chem. 26 (1987) 2524.
[133] R.L. Lord, F.A. Schultz, M.-H. Baik, Inorg. Chem. 49 (2010) 4611.
[134] J.J. Cruywagen, I.F.J. van der Merwe, J. Chem. Soc., Dalton Trans. (1987) 1701.
[135] G.K. Schweitzer, L.L. Pesterfield, The Aqueous Chemistry of the Elements, Oxford University Press, Oxford, 2010, p. 301.
[136] J.J. Cruywagen, Inorg. Chem. 19 (1980) 552.
[137] G. Schwarzenbach, G. Geier, J. Littler, Helv. Chim. Acta 45 (1962) 2601.
[138] A.R. Bowen, H. Taube, Inorg. Chem. 13 (1974) 2245.
[139] D.T. Richens, A.G. Sykes, Inorg. Syn. 23 (1985) 130.
[140] M. Segawa, Y. Sasaki, J. Am. Chem. Soc. 107 (1985) 5565.
[141] C. Sharp, E.F. Hills, A.G. Sykes, J. Chem. Soc., Dalton Trans. (1987) 2293.
[142] C.A. Routledge, A.G. Sykes, J. Chem. Soc., Dalton Trans. (1992) 325.
[143] M.N. Sokolov, N. Coichev, H.D. Moya, R. Hernandez-Molina, C.D. Borman, A.G. Sykes, J. Chem. Soc., Dalton Trans. (1997) 1863.
[144] M. Sokolov, D.N. Dybtsev, A.V. Virovets, V.P. Fedin, P. Esparza, R. Hernandez-Molina, D. Fenske, A.G. Sykes, Inorg. Chem. 41 (2002) 1136.
[145] A.F. Lindmark, Inorg. Chem. 31 (1992) 3507.
[146] A. Pidcock, B.W. Taylor, J. Chem. Soc. (A) (1967) 877.
[147] K.M. Al-Kathumi, L.A.P. Kane-Maguire, J. Chem. Soc., Dalton Trans. (1973) 1683.
[148] J.E. Pardue, M.N. Memering, G.R. Dobson, J. Organometal. Chem. 71 (1974) 407.
[149] J.R. Graham, R.J. Angelici, J. Am. Chem. Soc. 87 (1965) 5590.
[150] Y.-L. Shi, Y.-C. Gao, Q.-Z. Shi, D.L. Kershner, F. Basolo, Organometallics 6 (1987) 1528.
[151] L. Helm, A.E. Merbach, Chem. Rev. 105 (2005) 1923.
[152] D.T. Richens, Chem. Rev. 105 (2005) 1961.
[153] G. Powell, D.T. Richens, Inorg. Chem. 32 (1993) 4021.
[154] J. San Filippo Jr., M.A.S. King, Inorg. Chem. 15 (1976) 1228.
[155] R. Saillant, J.L. Hayden, R.A.D. Wentworth, Inorg. Chem. 6 (1967) 1497.
[156] A.B. Soares, R.C. Taylor, A.G. Sykes, J. Chem. Soc., Dalton Trans. (1980) 1101.
[157] Y. Sakaki, R.S. Taylor, A.G. Sykes, J. Chem. Soc., Dalton Trans. (1975) 396.
[158] P. Kathirgamanathan, A.B. Soares, A.G. Sykes, Inorg. Chem. 24 (1985) 2950.
[159] B.-L. Ooi, A.L. Petrou, A.G. Sykes, Inorg. Chem. 27 (1988) 3626.
[160] G.R. Cayley, R.S. Taylor, R.K. Wharton, A.G. Sykes, J. Chem. Soc., Dalton Trans. (1977) 1377.
[161] C. Sharp, A.G. Sykes, Inorg. Chem. 27 (1988) 501.
[162] R.K. Wharton, J.F. Ojo, A.G. Sykes, J. Chem. Soc., Dalton Trans. (1975) 1526.
[163] B.-L. Ooi, A.G. Sykes, Inorg. Chem. 27 (1988) 310.
[164] A. Majumdar, K. Pal, K. Nagarajan, S. Sarkar, Inorg. Chem. 46 (2007) 6136.
[165] M. Draganjac, E. Simhon, L.T. Chan, M. Kanatzidis, N.C. Baenziger, D. Coucouvanis, Inorg. Chem. 21 (1982) 3321.
[166] S.A. Cohen, E.I. Stiefel, Inorg. Chem. 24 (1985) 4657.
[167] W.-H. Pan, T.R. Halbert, L.L. Hutchings, E.I. Stiefel, J. Chem. Soc., Chem. Commun. (1985) 927.
[168] C.A. McConnachie, E.I. Stiefel, Inorg. Chem. 38 (1999) 964.
[169] E.I. Stiefel (Ed.), Dithiolene Chemistry: Synthesis, Properties, and Applications, Progress in Inorganic Chemistry, vol. 52, John Wiley and Sons Inc., New Jersey, 2004.
[170] T.B. Rauchfuss, Prog. Inorg. Chem. 52 (2004) 1.
[171] J.A. McCleverty, Prog. Inorg. Chem. 10 (1968) 49.
[172] H. Sugimoto, M. Harihara, M. Shiro, K. Sugimoto, K. Tanaka, H. Miyake, H. Tsukube, Inorg. Chem. 44 (2005) 6386.
[173] U. Ryde, C. Schulzke, K. Starke, J. Biol. Inorg. Chem. 14 (2009) 1053.
[174] F.J. Hine, A.J. Taylor, C.D. Garner, Coord. Chem. Rev. 254 (2010) 1570.
[175] M.A. Ansari, J. Chandrasekaran, S. Sarkar, Inorg. Chim. Acta 133 (1987) 133.
[176] R. Maiti, K. Nagarajan, S. Sarkar, J. Mol. Struct. 656 (2009) 169.
[177] A. Majumdar, K. Pal, S. Sarkar, J. Am. Chem. Soc. 128 (2006) 4196.
[178] A. Majumdar, K. Pal, S. Sarkar, Inorg. Chem. 47 (2008) 3393.
[179] A. Majumdar, K. Pal, S. Sarkar, Dalton Trans. (2009) 1927.
[180] H. Sugimoto, R. Tajima, T. Sakurai, H. Ohi, H. Miyake, S. Itoh, H. Tsukube, Angew. Chem. Int. Ed. 45 (2006) 3520.
[181] H. Sugimoto, H. Tano, K. Toyota, R. Tajima, H. Miyake, I. Takahashi, S. Hirota, S. Itoh, J. Am. Chem. Soc. 132 (2010) 8.
[182] R.H. Holm, Chem. Rev. 87 (1987) 1401.
[183] R.H. Holm, Coord. Chem. Rev. 100 (1990) 183.
[184] J.H. Enemark, C.G. Young, Adv. Inorg. Chem. 40 (1994) 1.
[185] C.G. Young, Biomimetic chemistry of molybdenum, in: B. Meunier (Ed.), Biomimetic Oxidations Catalyzed by Transition Metal Complexes, World Scientific Publishing Co., Singapore, 2000, p. 415.
[186] P.K. Chaudhury, K. Nagarajan, P. Dubey, S. Sarkar, J. Inorg. Biochem. 98 (2004) 1667.
[187] H.-K. Li, C. Temple, K.V. Rajagopalan, H. Schindelin, J. Am. Chem. Soc. 122 (2000) 7673.
[188] G.N. George, J. Hilton, C. Temple, R.C. Prince, K.V. Rajagopalan, J. Am. Chem. Soc. 121 (1999) 1256.
[189] G.N. George, K.J. Nelson, H.H. Harris, C.J. Doonan, K.V. Rajagopalan, Inorg. Chem. 46 (2007) 3097.
[190] M. Czjzek, J.-P. Dos Santos, J. Pommier, V. Méjean, R. Haser, J. Mol. Biol. 284 (1998) 435.
[191] L. Zhang, K.J. Nelson, K.V. Rajagopalan, G.N. George, Inorg. Chem. 47 (2008) 1074.
[192] K.-M. Sung, R.H. Holm, J. Am. Chem. Soc. 124 (2002) 4312.
[193] H. Sugimoto, S. Tatemoto, K. Suyama, H. Miyake, R. Mtei, S. Itoh, M.L. Kirk, Inorg. Chem. 49 (2010) 5368.
[194] M.J. Maher, J. Santini, I.J. Pickering, R.C. Prince, J.M. Macy, G.N. George, Inorg. Chem. 43 (2004) 402.
[195] J.M. Dias, M.E. Than, A. Humm, R. Huber, G.P. Bourenkov, H.D. Bartunik, S. Bursakov, J. Calvete, J. Caldeira, C. Carneiro, J.J.G. Moura, I. Moura, M.J. Romão, Structure 7 (1999) 65.
[196] M.G. Bertero, R.A. Rothery, M. Palak, C. Hou, D. Lim, F. Blasco, J.H. Weiner, N.C.J. Strynadka, Nat. Struct. Biol. 10 (2003) 681.
[197] P.J. Ellis, T. Conrads, R. Hille, P. Kuhn, Structure 9 (2001) 125.
[198] T. Conrads, C. Hemann, G.N. George, I.J. Pickering, R.C. Prince, R. Hille, J. Am. Chem. Soc. 124 (2002) 11276.
[199] H. Sugimoto, M. Tarumizu, H. Miyake, H. Tsukube, Eur. J. Inorg. Chem. (2008) 4494.
[200] S. Sarkar, S.K. Das, Proc. Indian Acad. Sci. (Chem. Sci.) 104 (1992) 437.

[201] J. Yadav, S.K. Das, S. Sarkar, J. Am. Chem. Soc. 119 (1997) 4315.
[202] R.A. Schmitz, M. Richter, D. Linder, R.K. Thauer, Eur. J. Biochem. 207 (1992) 559.
[203] R.A. Schmitz, S.P.J. Albracht, R.K. Thauer, Eur. J. Biochem. 209 (1992) 1018.
[204] P.A. Bertram, R. Schmitz, D. Linder, R.K. Thauer, Arch. Microbiol. 161 (1994) 220.
[205] L.J. Stewart, S. Bailey, B. Bennett, J.M. Charnock, C.D. Garner, A.S. McAlpine, J. Mol. Biol. 299 (2000) 593.
[206] J. Buc, C.-L. Santini, R. Giordani, M. Czjzek, L.-F. Wu, G. Giordano, Mol. Microbiol. 32 (1999) 159.
[207] C.D. Garner, L.J. Stewart, Met. Ions Biol. Syst. 39 (2002) 699.
[208] A.S. McAlpine, A.G. McEwan, A.L. Shaw, S. Bailey, J. Biol. Inorg. Chem. 2 (1997) 690.
[209] P.-L. Hagedoorn, W.R. Hagen, L.J. Stewart, A. Docrat, S. Bailey, C.D. Garner, FEBS Lett. 555 (2003) 606.
[210] P.A. Bertram, M. Karrasch, R.A. Schmitz, R. Böcher, S.P.J. Albracht, R.K. Thauer, Eur. J. Biochem. 220 (1994) 477.
[211] B. Hedman, K.O. Hodgson, E.I. Solomon, J. Am. Chem. Soc. 112 (1990) 1643.
[212] E.I. Solomon, B. Hedman, K.O. Hodgson, A. Dey, R.K. Szilagyi, Coord. Chem. Rev. 249 (2005) 97.
[213] R.K. Szilagyi, B.S. Lim, T. Glaser, R.H. Holm, B. Hedman, K.O. Hodgson, E.I. Solomon, J. Am. Chem. Soc. 125 (2003) 9158.
[214] E. van Lenthe, E.J. Baerends, J.G. Snijders, J. Chem. Phys. 99 (1999) 4597.
[215] W. Levason, R. Narayanaswamy, J.S. Ogden, A.J. Rest, J.W. Turff, J. Chem. Soc., Dalton Trans. (1981) 2501.
[216] A.L. Tenderholt, R.K. Szilagyi, R.H. Holm, K.O. Hodgson, B. Hedman, E.I. Solomon, Inorg. Chem. 47 (2008) 6382.
[217] A.L. Tenderholt, J.-J. Wang, R.K. Szilagyi, R.H. Holm, K.O. Hodgson, B. Hedman, E.I. Solomon, J. Am. Chem. Soc. 132 (2010) 8359.
[218] J.P. McNamara, I.H. Hillier, T.S. Bhachu, C.D. Garner, J. Chem. Soc., Dalton Trans. (2005) 3572.